Mon. Not. R. Astron. Soc. **000**, 000–000 (0000) Printed 11 January 2010 (MN LATEX style file v2.2)

arXiv:1001.1630v1 [astro-ph.CO] 11 Jan 2010

# The radio properties of a complete, X-ray selected sample of nearby, massive elliptical galaxies

R.J.H.Dunn[1,2⋆]†, S.W.Allen[3,4], G.B.Taylor[5]‡, K.F.Shurkin[5], G.Gentile[6,7]
A.C.Fabian[8] and C.S.Reynolds[9]
[1] Excellence Cluster “Universe”, Technische Universität München, Boltzmannstrasse 2, D-85748, Garching, Germany
[2] School of Physics and Astronomy, Southampton, University of Southampton, SO17 1BJ
[3] Kavli Institute for Particle Astrophysics and Cosmology at Stanford University, 452 Lomita Mall, Stanford, CA 94305-4085, USA
[4] SLAC National Accelerator Laboratory, 2575 Sand Hill Road, Menlo Park, CA 94025, USA
[5] University of New Mexico, Department of Physics and Astronomy, Alberquerque, NM 87131, USA.
[6] Institut d’Astronomie et d’Astrophysique, Université Libre de Bruxelles, CP 226, Boulevard du Triomphe, B-1050 Bruxelles, Belgium
[7] Sterrenkundig Observatorium, Universiteit Gent, Krijgslaan 281, B-9000 Gent, Belgium
[8] Institute of Astronomy, Madingley Road, Cambridge, CB3 0HA
[9] Department of Astronomy and the Maryland Astronomy Center for Theory and Computation, University of Maryland, College Park, MD 20742, USA

11 January 2010

**ABSTRACT**

We investigate the radio properties of a complete sample of nearby, massive, X-ray bright elliptical and S0 galaxies. Our sample contains 18 galaxies with ROSAT All-Sky Survey X-ray fluxes $F_{\rm X,\,0.1-2.4\,keV} > 3\times10^{-12}\,{\rm erg\,s^{-1}\,cm^{-2}}$, within a distance of $100\,{\rm Mpc}$. For these galaxies, we have complete (18/18) VLA radio and Chandra X-ray coverage. Nuclear radio emission is detected from 17/18 of the galaxies. Ten of the galaxies exhibit extended radio emission; of these ten, all but one also exhibit clear evidence of interaction of the radio source with the surrounding, X-ray emitting gas. Among the seven galaxies with unresolved radio sources, one has clear, and one has small, cavity-like features in the *Chandra* X-ray images; a third has a disturbed X-ray morphology. Using a radio luminosity limit equivalent to $L_{1.4\,{\rm GHz}} > 10^{23}{\rm W\ Hz^{-1}}$ to calculate the radio-loud fraction, we find that this misses the majority of the radio detected galaxies in the sample. We determine integrated radio-to-X-ray flux ratios for the galaxies, $\mathcal{GR}_{\rm X}$, which are shown to span a large range (factor of 100). We calculate the mass-weighted cooling times within $1\,{\rm kpc}$, and find hints for an anticorrelation with the radio luminosity. We also calculate limits on $k/f$, where $k$ is the ratio of the total particle energy to that of relativistic electrons radiating in the range $10\,{\rm MHz}$–$10\,{\rm GHz}$ and $f$ is the volume filling factor of the plasma in the cavity. The $k/f$ distribution is also broad, reflecting previous results for larger galaxy clusters. Lowering the X-ray flux limit, at the expense of less complete VLA and Chandra coverage, increases the size of our sample to 42 galaxies. Nuclear radio activity is detected in at least 34/42 of this extended sample.

**Key words:** galaxies: active, galaxies: lenticular and elliptical, cD, galaxies: jets

## 1 INTRODUCTION

Super-massive black holes (SMBH) appear to be common in massive galaxies (see e.g. Richstone 1998; Ferrarese & Merritt 2000; Kormendy 2001; Ferrarese 2002). A question of significant interest is the level to which these SMBHs are active i.e. their emitted power as a fraction of accretion rate or Eddington luminosity (Best et al. 2005; Nagar et al. 2005; Chiaberge et al. 2005; Balmaverde & Capetti 2006; Capetti & Balmaverde 2006; Filho et al. 2006; Gallo et al. 2008). Generally, power is released from active galactic nuclei (AGN) in either radiative or kinetic forms. Whereas the radiated power is straightforward to measure, using observations across the electromagnetic spectrum, determining the kinetic power of AGN is more challenging, particularly for low-to-moderate mass galaxies and SMBHs. For the highest mass galaxies, however, and in particular those at the centers of clusters and groups, nature provides powerful, additional tools to probe AGN and their impact on their environments.

Within massive elliptical galaxies, groups and clusters, embedded AGN have been shown to interact strongly with the sur-

---

⋆ E-mail: robert.dunn@ph.tum.de
† Alexander von Humboldt Fellow
‡ Adjunct Astronomer at the National Radio Astronomy Observatory

© 0000 RAS

rounding hot X-ray emitting medium. This interaction causes disturbances seen as shocks, ripples, and cavities (e.g. Fabian et al. 2000, 2003, 2006; Forman et al. 2005). The cavities, which are filled with low-density, radio-emitting, relativistic plasma, appear as X-ray surface brightness depressions – a consequence of the X-ray luminous, thermal gas being displaced by the jets of the AGN. X-ray cavities, filled with radio emitting plasma, are clearly associated with the central AGN of nearby clusters such as Perseus (e.g. ., Böhringer et al. 1993; Fabian et al. 2000, 2003, 2006), Virgo (e.g. Churazov et al. 2001; Forman et al. 2005), Centaurus (e.g. Taylor et al. 2006) and Hydra A (e.g. McNamara et al. 2000).

Crucially, studies of cavities allow the total kinetic energy and kinetic power injected by AGN into their surroundings to be estimated (e.g. Churazov et al. 2002; Allen et al. 2006; Bîrzan et al. 2004; Rafferty et al. 2006; Dunn & Fabian 2006, 2008). This injection is energetically sufficient to prevent catastrophic cooling of the X-ray emitting gas, providing a potential solution to the puzzle of why most nearby, massive galaxies appear 'red and dead' (Bower et al. 2006; Croton et al. 2006a,b; Somerville et al. 2008). For a review of the effect SMBHs have on their host galaxy's evolution see Cattaneo et al. (2009).

Dunn & Fabian (2006, 2008) showed that almost all galaxies at the centers of nearby clusters for which the central cooling time of the X-ray emitting gas is short (i.e. $t_{\rm cool} << t_{\rm H}$), and for which this gas would otherwise cool rapidly and form stars, host powerful, radio-emitting AGN and X-ray cavities, this extended the work of Burns (1990) who showed that 70 per cent of dominant galaxies in rich clusters with cooling cores are radio loud. Using a larger sample of clusters and groups, Sun (2009) argue the inverse, that all brightest cluster galaxies with radio AGN have cool cores. As radio-emitting AGN are seen in almost all clusters with short cooling times, the duty cycle of these AGN must be high.

It is important to recognise, however, that the radio sources at the centres of clusters are in extreme environments. To assess the impact of such processes on the general population of massive galaxies, it is essential to extend this work to the general population of massive ellipticals. Recent studies have used the SDSS[1] (York et al. 2000; Stoughton et al. 2002) and the NVSS [2] (Condon et al. 1998) to examine the fraction of galaxies with radio-loud AGN. Best et al. (2005) combine these two surveys, and select galaxies with redshifts between $0.03 < z < 0.1$. They show that the fraction of galaxies with a radio-loud AGN depends on the stellar mass of the galaxy; the maximum fraction is between 30 and 40 per cent, significantly below that inferred for nearby clusters. (Note that the 'maximum' fraction is obtained for the least restrictive constraint on the radio luminosity and the largest galaxies in that study.) Other investigations into the fraction of actively accreting SMBHs in the nearby Universe have led to similar results, though do not rule out the possibility of significantly larger fractions for lower radio luminosity thresholds (see e.g. Nagar et al. 2005; Chiaberge et al. 2005; Balmaverde & Capetti 2006; Capetti & Balmaverde 2006; Filho et al. 2006).

Another angle has been taken by Goulding & Alexander (2009) who select very local ($D < 15\,{\rm Mpc}$) galaxies which are bolometrically luminous using infra-red observations. In this volume limited sample (94 per cent complete) of the 64 galaxies, 17 host an AGN (27 per cent).

In this paper we use high quality X-ray and radio observations to determine the fraction of active AGN in a complete sample of nearby, massive elliptical galaxies, selected to have high optical and X-ray fluxes and lie within a distance of 100Mpc. Our sample includes both dominant galaxies at the centres of groups and clusters and field ellipticals with their own halos of hot X-ray gas. We show that the fraction of galaxies that are active, i.e. exhibit radio emission and/or clear X-ray cavities associated with a central AGN is very high: $\gtrsim 90$ per cent. We also investigate the prevalence of cool cores within this sample.

Our discussion will proceed as follows. We begin in Section 2 with a description of the sample and selection criteria. In Section 3, we describe the radio data selection and processing. In Section 4, we describe the X-ray data reduction and preparation. In Section 5, we discuss individual sources and in Section 6, we conduct a population study. Section 7 extends some aspects of the analysis to a larger sample of galaxies, at the expense of incomplete VLA and Chandra coverage. We conclude in Section 9.

Throughout this paper, we assume a standard flat $\Lambda$CDM cosmology with $H_0$=70 km s$^{-1}$ Mpc$^{-1}$ and $\Omega_{\rm m} = 0.3$.

## 2 SAMPLE SELECTION

Our study is focused on a clearly defined and essentially complete sample of nearby elliptical galaxies with measured optical, X-ray and radio properties. We start from the catalogue of Beuing et al. (1999). The northern part of this catalogue contains all E and E/S0 galaxies from the study of Faber et al. (1989) with $\delta \geqslant 0^\circ$ and magnitudes brighter than $B_{\rm T} = 13.5$ mag. The southern part of the Beuing et al. (1999) catalogue is drawn from Bender et al. (1989); it contains all E and E/S0 galaxies with $\delta < 0^\circ$ and $B_{\rm T} < 13.5$ mag from (Faber et al. 1989), as well as galaxies from the ESO Lauberts-Valentijn Catalogue (Lauberts & Valentijn 1989) brighter than $B_{\rm T} = 13.5$ mag and with morphological type $T_{\rm old}$ or $T_{\rm new} \leqslant -3$. In addition, the catalogue includes galaxies with $\delta \geqslant 0^\circ$, $B_{\rm T} < 13.7$ and numerical class $T \leqslant -3$ from the Third Reference Catalogue for Bright Galaxies (de Vaucouleurs et al. 1991) and the Tully Nearby Galaxies Catalogue (Tully 1988)[3,4].

The sample of Beuing et al. (1999) contains 530 early type galaxies; 313 in the southern and 217 in the northern parts. The distribution of galaxies of different types is as follows: 49 per cent ellipticals ($T = -5$), one of which is a compact elliptical ($T = -6$); 15 per cent cD-type galaxies ($T = -4$); 26 per cent E/S0a ($T = -3$); 7 per cent S0s ($T = -2$); and 3 per cent later types (de Vaucouleurs et al. 1991). From their magnitude-distribution function, Beuing et al. (1999) judge that their sample starts to become incomplete at $B_{\rm T} \approx 13.0$. However they state that it is still 90 per cent complete at $B_{\rm T} = 13.5$, assuming a spatially homogeneous distribution.

Beuing et al. (1999) provide X-ray luminosities, or upper limits on the X-ray luminosity, for 293 galaxies in their sample, based on data from the ROSAT[5] All-Sky Survey (RASS). They exclude galaxies which are not at the centre of the bright X-ray emission, but embedded in it, *unless* they clearly stand out against it. The upper limits obtained for some galaxies were classed as meaningless if they resulted from short exposures, or if the galaxy has a distance $> 43h_{70}^{-1}\,\mathrm{Mpc}$. Their final sample consists of all normal galaxies showing individual emission, as well as galaxies at the centres of clusters and groups, if the X-ray emission is centred on the galaxy and reasonably symmetric around it. O'Sullivan et al. (2001) updated these $L_{\rm X}$ values, also incorporating pointed, follow-up X-ray observations made with the ROSAT Position Sensitive Proportional Counter (PSPC), where available. For our sample selection, we use the X-ray luminosities of O'Sullivan et al. (2001), converted to our reference cosmology. 207 galaxies in the O'Sullivan et al. (2001) study have X-ray luminosity measurements as opposed to upper limits.

---

[1] Sloan Digital Sky Survey

[2] NRAO (National Radio Astronomy Observatory) VLA (Very Large Array) Sky Survey

[3] Beuing et al. (1999) adopt a fainter $B_{\rm T}$ threshold for the de Vaucouleurs et al. (1991) and Tully (1988) catalogues, since de Vaucouleurs et al. (1991) found hints of a zero-point offset of $0.12 - 0.18$ mag.

[4] The numerical class constraint excludes at least one well known X-ray bright galaxy, NGC 1275, as it is classed as a peculiar galaxy, $T = 99$

From the initial catalogue of optically bright galaxies with X-ray luminosity measurements, we identify all galaxies with $0.1 - 2.4$keV fluxes $> 3 \times 10^{-12}\,\mathrm{erg\,s^{-1}\,cm^{-2}}$. We also impose an upper distance limit of 100 Mpc. Together, these two criteria ensure that all galaxies studied should be sufficiently X-ray bright and nearby to allow the properties of their diffuse, X-ray emitting gas to be studied in detail with Chandra.

We note that the X-ray luminosities reported by O'Sullivan et al. (2001) are total luminosities, including the contributions from X-ray binaries, AGN and other compact sources, as well as the hot, gaseous components. For the largest elliptical galaxies the contributions from binaries is expected to be minimal (see e.g. Kim & Fabbiano 2004; Humphrey et al. 2008; Brough et al. 2008). As we show in this paper, the impact of the central AGN on the total X-ray emission is also typically low. Only in $\sim 10$ per cent (2/18) of our galaxies does the AGN outshine the diffuse gas at X-ray wavelengths (see Sections 5 and 6.1)[6] For the other galaxies, the X-ray emission from the central AGN typically accounts for less than 1 per cent of the total.

The X-ray properties of the parent sample and X-ray flux and distance cuts are shown in Fig. 1. The resulting sample consists of 18 galaxies, which are detailed in Table 1. VLA radio data and *Chandra* X-ray observations are available for all 18 targets.

Two of the eighteen sources, IC 310 and NGC 4203, are anomalous in that their X-ray emission is dominated by the central AGN[7] These two galaxies are the two most late type (S0) galaxies in the sample (Table 1). For these reasons, although IC 310 and NGC 4203 formally meet the optical, X-ray and distance selection criteria, we flag or exclude them from certain population studies.

## 3 RADIO DATA

The radio data for the targets were obtained from the NRAO VLA archive.[8] Multiple observations of each source are available, for various wavelengths and configurations. For each source we select and present the radio map best suited to the present purposes.

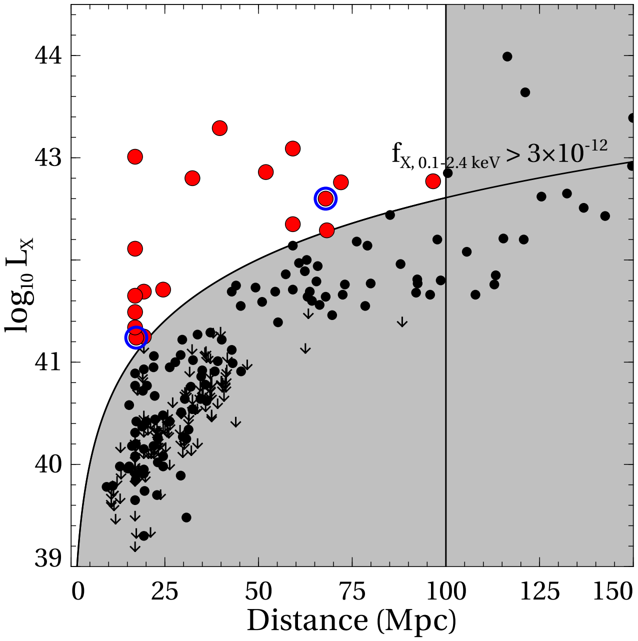

**Figure 1.** The distance-luminosity distribution of the galaxy sample of Beuing et al. 1999 with the flux and distance cuts used to obtain our final sample. The 18 galaxies in our sample are highlighted in red. Galaxies for which only upper limits on the X-ray luminosity are available are shown with arrows. IC 310 and NGC 4203, for which the X-ray emission is dominated by the central AGN, are highlighted with blue circles. The X-ray luminosities shown are taken from O'Sullivan et al. (2001) but converted to $H_0 = 70\,\mathrm{km\,s^{-1}\,Mpc^{-1}}$.

In selecting the data to be analysed, preference was given to more recent observations, and to those with time on source $\geqslant 5$ minutes. As steep spectrum emission is brighter at lower frequencies, preference was also given to observations performed at 1.5 GHz. In addition, A-configuration observations at 1.5 GHz, or B-configuration observations at 5 GHz were desirable in order to provide arcsecond resolution for comparison with X-ray images from *Chandra*.

The data were reduced in the standard manner using AIPS[9](Greisen 2003). After an initial editing of the data, absolute amplitude and phase calibration were performed on each dataset using the scripts VLAPROCS and VLARUN. For datasets in which the flux calibrator was resolved, a model was used (if available) for the calibration. If bad data were still present after the initial calibration, those data were flagged and the calibration was repeated.

An image of each source was created using the task IMAGR. Side-lobes from outlying sources were removed by using multiple facets while imaging. Proper placement of the facets was determined using the task SETFC, which was set up to search a 0.5 degree radius for sources in the NVSS catalogue with flux $\geqslant 10$ mJy. Typically, sources outside of that range are either not bright enough or too far from the pointing centre to have an appreciable effect on the quality of the image. In any event in which SETFC failed to include significant sources, facet positions were set manu-

---

[5] Röntgen Satellit (*ROSAT*)

[6] Two of the eighteen sources, IC 310 and NGC 4203, are anomalous in that their X-ray emission is dominated by their central AGN. These two galaxies are also the two most late-type (S0) galaxies in the sample (see Table 1). For these reasons, although IC 310 and NGC 4203 formally meet the optical, X-ray and distance selection criteria, we flag or exclude them from certain population studies.

[7] The X-ray luminosities of O'Sullivan et al. (2001). include the contributions of point sources in the galaxies.

[8] The VLA (Very Large Array) is operated by the National Radio Astronomy Observatory (NRAO). The National Radio Astronomy Observatory is operated by Associated Universities, Inc., under cooperative agreement with the National Science Foundation.

[9] Astronomical Image Processing System

**Table 1.** The Sample

| Source | Alternate Name | RA$^a$ J2000 | Dec$^a$ J2000 | Redshift$^a$ | Distance Mpc | Type$^b$ | | $\log(L_{\rm X})$ erg s$^{-1}$ |
|---|---|---|---|---|---|---|---|---|
| IC 310 | — | 03h 16m 43.00s | +41d 19m 29.4s | 0.018940 | 67.92 | -2.0 | - | 42.60 |
| IC 1860 | — | 02h 49m 33.7s | -31d 11m 21s | 0.022902 | 96.59 | -4.7 | BCG | 42.77 |
| NGC 499 | — | 01h 23m 11.5s | +33d 27m 38s | 0.014673 | 59.15 | -2.8 | - | 42.35 |
| NGC 507 | — | 01h 23m 40.0s | +33d 15m 20s | 0.016458 | 71.99 | -3.2 | - | 42.76 |
| NGC 533 | — | 01h 25m 31.36s | +01d 45m 32.8s | 0.018509 | 68.23 | -4.8 | - | 42.29 |
| NGC 708 | A262 | 01h 52m 46.48s | +36d 09m 06.6s | 0.016195 | 59.15 | -4.8 | BCG | 43.09 |
| NGC 1399 | — | 03h 38m 29.08s | -35d 27m 02.7s | 0.004753 | 19.40 | -4.2 | BCG | 41.69 |
| NGC 1404 | — | 03h 38m 51.92s | -35d 35m 39.8s | 0.006494 | 19.40 | -4.7 | - | 41.25 |
| NGC 1550 | — | 04h 19m 37.93s | +02d 24m 35.7s | 0.012389 | 51.95 | -3.9 | - | 42.86 |
| NGC 4203 | — | 12h 15m 05.06s | +33d 11m 50.38s | 0.003623 | 17.38 | -2.7 | - | 41.24 |
| NGC 4406 | M 86 | 12h 26m 11.74s | +12d 56m 46.40s | -0.000814 | 17.06 | -4.7 | - | 42.11 |
| NGC 4472 | M 49 | 12h 29m 46.76s | +08d 00m 01.71s | 0.003326 | 17.06 | -4.7 | - | 41.49 |
| NGC 4486 | M 87 | 12h 30m 49.4s | +12d 23m 28s | 0.004360 | 17.06 | -4.3 | BCG | 43.01 |
| NGC 4636 | — | 12h 42m 49.9s | +02d 41m 16s | 0.003129 | 17.06 | -4.8 | - | 41.65 |
| NGC 4649 | M 60 | 12h 43m 39.66s | +11d 33m 09.4s | 0.003726 | 17.06 | -4.6 | - | 41.34 |
| NGC 4696 | Centaurus Cluster | 12h 48m 49.3s | -41d 18m 40s | 0.009867 | 39.65 | -3.9 | BCG | 43.29 |
| NGC 5044 | — | 13h 15m 23.97s | -16d 23m 07.9s | 0.009020 | 32.36 | -4.8 | - | 42.80 |
| NGC 5846 | — | 15h 06m 29.29s | +01d 36m 20.24s | 0.005717 | 24.55 | -4.7 | - | 41.71 |

The sample of galaxies. $^a$ Positions and redshifts obtained from NASA/IPAC Extragalactic Database (NED). $^b$ The Type shows the $T$-type de Vaucouleurs et al. (1991) with E=-5, E/S0=-3, S0=-2, S0a=0. Also shown is whether the galaxy is a Brightest Cluster Galaxy, (BCG), defined as the galaxy (likely) to be the dominant one in a cluster listed in the Abell catalogues (Abell 1958; Abell et al. 1989). Also listed are the total X-ray luminosities (Section 2).

ally. For those sources with sufficient signal-to-noise ratios, imaging and phase-only self-calibration were then performed iteratively, until the theoretical noise was reached or until the quality of the map ceased to benefit from the iterations. Observational parameters and data for the VLA observations are tabulated in Table 2.

For NGC 1404 the VLA radio map from 2007 shows a faint point source coincident with the galaxy centre. However the detection is only just above the level of the noise in the data, and so cannot be determined accurately. The NVSS catalogue also lists a source at the location of NGC 1404. We list this detection separately in Table 2. During the analysis of the radio data for NGC 4472 we found that the data from the A configuration has a $(u, v)$ coverage such that the large scale emission was not detected. As a result of this, we checked all other A-configuration observations for undetected large scale emission using C-configuration data present in the VLA Archive. This problem was not found in any other galaxy apart from NGC 4472.

The reduction and analysis of the $1.5\,{\rm GHz}$ radio data for NGC 4486 are described by Hines et al. (1989).

## 4 X-RAY DATA REDUCTION

The *Chandra* X-ray data were cleaned and reprocessed using the CIAO software and latest calibration files (CIAO v4.1.2, CALDB v4.1.1). Hot pixels and cosmic ray afterglows were identified and excluded. Charge-Transfer Inefficiency was corrected for and standard grade selection applied. Light curves were generated from relatively source-free regions of the detectors and used to screen the data for background flares. For observations made in Very Faint (VF) mode, the additional information available for identifying and screening background events was utilised. Background files were generated from the CALDB blank-field data-sets. These were processed in a similar manner to the target observations. The background data-sets were normalised by the ratio of the $9-12\,{\rm keV}$ count rates in the source and background data-sets. Point-sources were identified using the WAVDETECT wavelet-transform procedure, and excluded.

To model other, possible background components not accounted for in the blank-sky fields, background spectra were also extracted from relatively source-free regions of the detectors (e.g. the ACIS-S1 chip for ACIS-S data) and compared with blank-sky fields. Any excess soft emission components so detected were fitted with a single temperature MEKAL model with a fixed solar abundance and scaled appropriately in the subsequent analysis. NGC 5846 exhibits clear excess soft background emission. Note, however, that care is required here since in many cases the emission from the cluster/group extends onto the S1 chip.

For each galaxy, concentric annular regions were selected to give approximately constant signal-to-noise in the $0.6-7.0$ keV band. Annuli were centered on the peak of the X-ray emission. Where the Chandra data revealed the presence of a central point source, the minimum radius was adapted to exclude it. The signal-to-noise ratio for the annuli was adjusted iteratively to obtain a number of regions ranging from 10 to 25.

The $0.6-7.0$ keV spectrum for each spherical shell was modelled as a single temperature plasma, using the MEKAL (e.g. Mewe et al. 1995) model, with a PHABS absorption model fixed to the galactic $N_{\rm H}$. The spectra for all annuli were modelled simultaneously to determine the deprojected gas temperature, metallicity and density profiles for the galaxies. The modified C-statistic available in XSPEC (Arnaud 1996, 2004) was used in all spectral fitting.

## 5 NOTES ON INDIVIDUAL SOURCES

Our sample is essentially unbiased with respect to the morphology of the X-ray emission from the galaxies. X-ray emission from the hot, diffuse gaseous halos and any AGN that may be present will both contribute to the measured X-ray flux. In this Section,

**Table 2.** VLA Data and Observational Parameters

| Source | Frequency ( GHz) | Config | Date | Time on Source (sec) | Peak Flux (Jy/beam) | Total Flux Density (Jy) | RMS ($\mu$Jy/beam) | Beam (arcsec) | PA (deg) |
|---|---|---|---|---|---|---|---|---|---|
| IC 310 | 4.885 | C | 1984 May 01 | 1170 | $1.36\times10^{-1}$ | $1.98\times10^{-1}$ | 73.9 | $3.99\times3.93$ | -43.55 |
| IC 1860 | 1.365 | A | 2007 Jun 08 | 8070 | $1.23\times10^{-2}$ | $1.39\times10^{-2}$ | 60.2 | $2.92\times1.42$ | 11.83 |
| NGC 499 | 1.365 | A | 2007 Jun 08 | 6070 | $<1.18\times10^{-4}$ | - | 35.8 | $1.43\times1.16$ | -62.60 |
| NGC 507 | 1.525 | C | 1984 May 14 | 1770 | $8.61\times10^{-3}$ | $8.45\times10^{-2}$ | 87.1 | $17.58\times12.11$ | -81.43 |
| NGC 533 | 4.885 | C | 1997 Jul 05 | 230 | $5.06\times10^{-3}$ | $8.91\times10^{-3}$ | 93.3 | $5.08\times4.60$ | -14.47 |
| NGC 708 | 1.365 | A | 2000 Dec 13 | 1520 | $6.57\times10^{-3}$ | $8.25\times10^{-2}$ | 55.5 | $1.46\times1.18$ | -49.36 |
| NGC 1399 | 1.465 | H[1] | 1983 Dec 16 | 27910 | $1.89\times10^{-2}$ | $4.63\times10^{-1}$ | 72.1 | $4.15\times2.80$ | 38.46 |
| NGC 1404 | 1.365 | A | 2007 Jun 08 | 6060 | $3.50\times10^{-4}$ | - | 85.8 | $3.64\times1.48$ | 10.82 |
| NGC 1550 | 1.365 | C | 1997 Sep 18 | 410 | $2.68\times10^{-3}$ | $1.27\times10^{-2}$ | 76.7 | $18.6\times16.8$ | -84.14 |
| NGC 4203 | 4.885 | A | 1999 Sep 05 | 423 | $1.66\times10^{-2}$ | $1.80\times10^{-2}$ | 93.6 | $0.48\times0.39$ | 63.12 |
| NGC 4406 | 4.885 | C | 1984 Jun 03 | 510 | $5.09\times10^{-4}$ | $4.91\times10^{-4}$ | 67.1 | $4.32\times3.86$ | 55.55 |
| NGC 4472 | 1.489 | C | 1986 Nov 26 | 192 | $1.19\times10^{-1}$ | $2.23\times10^{-1}$ | 250 | $17.19\times14.24$ | -37.6 |
| NGC 4486 | 1.466 | A | 1989 Mar 01 | 10020 | $1.74\times10^{0}$ | $1.38\times10^{1}$ | 32.5 | $0.80\times0.80$ | 0.00 |
| NGC 4636 | 1.425 | A | 2002 Mar 12 | 12440 | $4.80\times10^{-3}$ | $6.45\times10^{-2}$ | 45.8 | $1.42\times1.33$ | -18.42 |
| NGC 4649 | 1.465 | B | 1984 Jan 24 | 4410 | $1.72\times10^{-2}$ | $2.82\times10^{-2}$ | 29.7 | $4.51\times3.64$ | 44.76 |
| NGC 4696 | 1.565 | A | 1998 Apr 23 | 3635 | $3.58\times10^{-1}$ | $3.64\times10^{0}$ | 118 | $4.40\times2.09$ | 0.50 |
| NGC 5044 | 1.465 | A | 1992 Nov 27 | 8560 | $2.71\times10^{-2}$ | $2.99\times10^{-2}$ | 32.8 | $1.77\times1.03$ | -16.83 |
| NGC 5846 | 1.465 | A | 2002 Mar 12 | 9220 | $9.93\times10^{-3}$ | $1.02\times10^{-2}$ | 20.8 | $1.32\times1.18$ | -17.86 |
| NGC 1404[†] | 1.400 | D | 1993 Oct 07 | - | $3.42\times10^{-4}$ | $3.90\times10^{-4}$ | 450 | $45\times45$ | 0 |

[1] Hybrid configuration (A and B). [†] From NVSS,as the point source in the A-configuration image is only just above the noise.

**Table 3.** X-ray data parameters

| Source | Date | Obs ID | Detector | Mode | Exposure[1] | $N_{\rm H}^{\dagger}$ |
|---|---|---|---|---|---|---|
| IC 310 | 23 Dec 2004 | 5597 | ACIS-I | FAINT | 25.2 | 1.30 |
| IC 1860 | 12 Sep 2009 | 10537 | ACIS-S | VFAINT | 37.2 | 2.40 |
| NGC 499 | 4 Feb 2009 | 10865 | ACIS-S | VFAINT | 5.1 | 5.30 |
|  | 5 Feb 2009 | 10866 | ACIS-S | VFAINT | 8.0 | 5.30 |
|  | 7 Feb 2009 | 10867 | ACIS-S | VFAINT | 7.0 | 5.30 |
|  | 12 Feb 2009 | 10536 | ACIS-S | VFAINT | 18.4 | 5.30 |
| NGC 507 | 11 Oct 2000 | 2882 | ACIS-I | VFAINT | 43.6 | 5.24 |
| NGC 533 | 28 Jul 2002 | 2880 | ACIS-S | VFAINT | 34.8 | 3.10 |
| NGC 708 | 03 Aug 2001 | 7921 | ACIS-S | VFAINT | 110.6 | 5.37 |
| NGC 1399 | 18 Jan 2000 | 319 | ACIS-S | FAINT | 55.9 | 1.34 |
| NGC 1404 | 13 Feb 2003 | 2492 | ACIS-S | FAINT | 29.0 | 1.45 |
| NGC 1550 | 08 Jan 2002 | 5800 | ACIS-S | VFAINT | 44.5 | 11.50 |
| NGC 4203 | 10 Mar 2009 | 10535 | ACIS-S | VFAINT | 41.4 | 1.10 |
| NGC 4406 | 07 Apr 2000 | 318 | ACIS-S | FAINT | 12.6 | 2.62 |
| NGC 4472 | 12 Jun 2000 | 321 | ACIS-S | VFAINT | 29.6 | 1.66 |
| NGC 4486 | 05 Jul 2002 | 2707 | ACIS-S | FAINT | 98.4 | 2.54 |
| NGC 4636 | 26 Jan 2000 | 323 | ACIS-S | FAINT | 44.2 | 1.81 |
| NGC 4649 | 30 Jan 2007 | 8182 | ACIS-S | VFAINT | 49.2 | 2.20 |
|  | 20 Apr 2000 | 785 | ACIS-S | VFAINT | 19.4 | 2.20 |
| NGC 4696[2] | 01 Apr 2004 | 4954 | ACIS-S | FAINT | 88.0 | 8.06 |
| NGC 5044 | 19 Mar 2000 | 3225 | ACIS-S | VFAINT | 83.1 | 4.93 |
| NGC 5846 | 24 May 2000 | 788 | ACIS-S | FAINT | 22.1 | 4.26 |

[1] The final exposure in ks after all screening. [2] Also analysed in Taylor et al. (2006). [†] The Galactic column density, $N_{\rm H}$, is in units of $10^{20}$ $atom\,{\rm cm}^{-2}$ determined from HI studies (Dickey & Lockman 1990).

we discuss the X-ray and radio morphologies for the galaxies in the sample, comment on the presence of nuclear X-ray emission, and examine the evidence for interactions between the central radio sources and surrounding X-ray gas. Several of the galaxies in the sample have previously been studied by other authors.

### 5.1 IC 310

IC 310 is an S0 galaxy in the south-west region of the Perseus cluster. The radio morphology is that of a head-tail galaxy (e.g. Sijbring & de Bruyn 1998) with a bright core and extended tail of length around 400 kpc. Our data show the radio tail disconnected from the much brighter head. There is only an observation

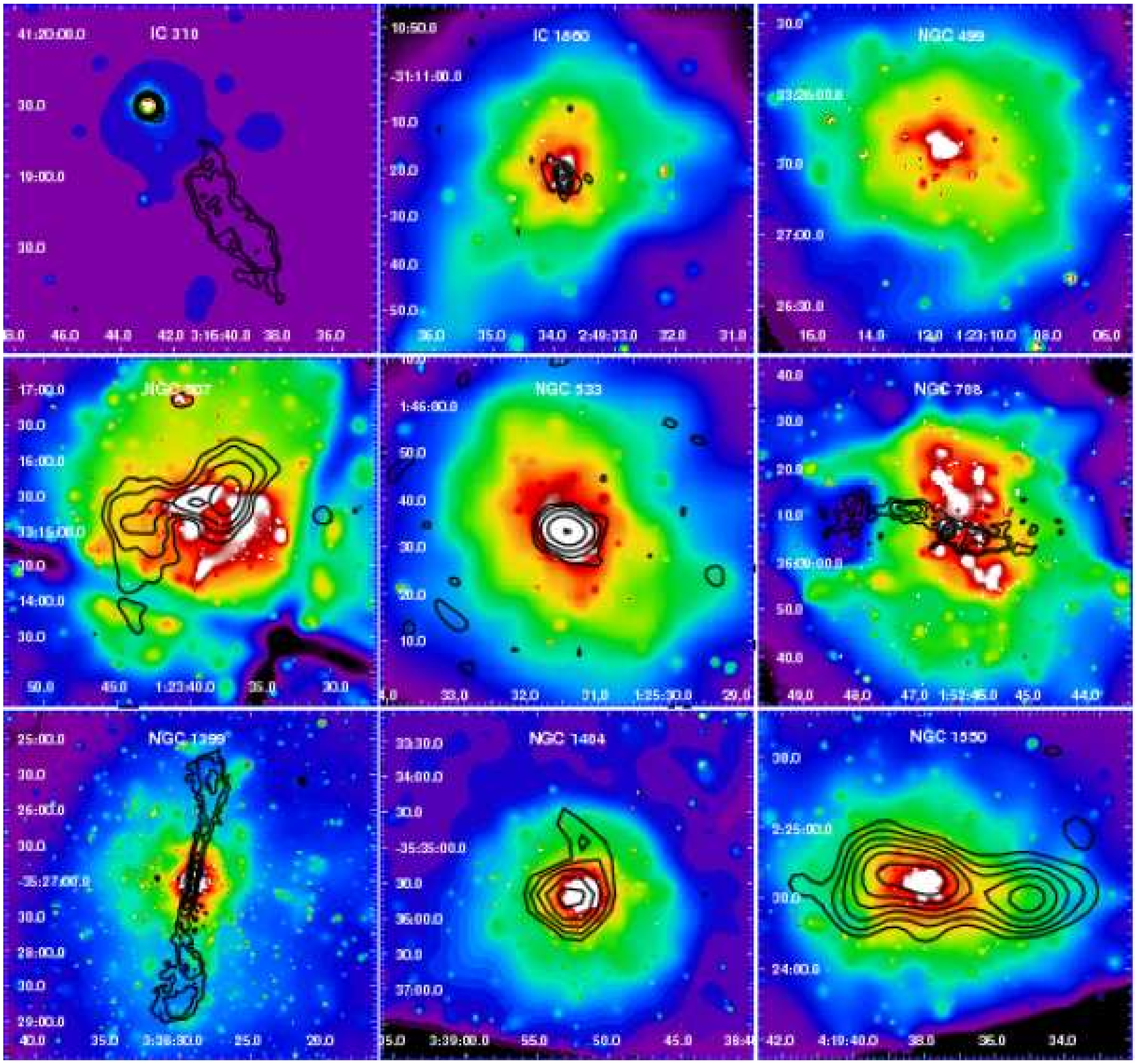

**Figure 2.** Adaptively smoothed X-ray images (black/purple for faint emission, red/white for bright emission) with radio contours overlaid. From top left to bottom right: IC 310, IC 1860, NGC 499, NGC 507, NGC 533, NGC 708, NGC 1399, NGC 1404 and NGC 1550. The Chandra image of NGC507 also shows artefacts associated with chip gaps in the ACIS-I array. The radio contours for NGC 1404 are those from the NVSS survey.

at $4.9$ GHz which has sufficient resolution to show the structure of the source.

The X-ray emission is dominated by a central point source, coincident with the radio core. The extended X-ray halo is faint, reflecting the relatively late-type nature of the galaxy. A small X-ray extension is observed in the same direction as the radio tail. The current data do not allow any detailed study of interactions between the radio and X-ray emitting plasmas.

### 5.2 IC 1860

IC 1860 is the dominant galaxy of the IC 1860 group, which is itself part of Abell S301. The dominant galaxy of Abell S301 according to Hudson et al. (2001) is the Seyfert 2 galaxy IC 1859, which is 6.5 arcminutes distant from IC 1860. However, *XMM-Newton* data (Observation 0146510401) shown in Fig. 2, IC 1860 sits at the peak of the diffuse X-ray emission, and the position of IC 1859 is off to the west.

The radio data of IC 1860 show a clear point source with faint extensions in the northeast and southwest directions. The X-ray data show an extension towards the southeast. However there is no clear correlation between the faint radio extensions and the X-ray gas.

### 5.3 NGC 499

NGC 499 lies near NGC 507 in the NGC 507 galaxy Group. There is no radio detection for this galaxy down to a level of $1.18 \times 10^{-4}$ Jy, identifying NGC 499 as abnormally radio quiet for its X-ray luminosity. The RMS noise in the VLA data is $35.8$ $\mu$Jy/beam, which is fairly typical of the observations presented here (see Table 2). There appears to be a depression in the X-ray emission to the south-east, visible in Fig. 2. However, whether this is the result of a past outburst of AGN activity is not clear. Kim & Fabbiano (1995); Paolillo et al. (2003) report evidence for tidal interactions between NGC 499 and NGC 507.

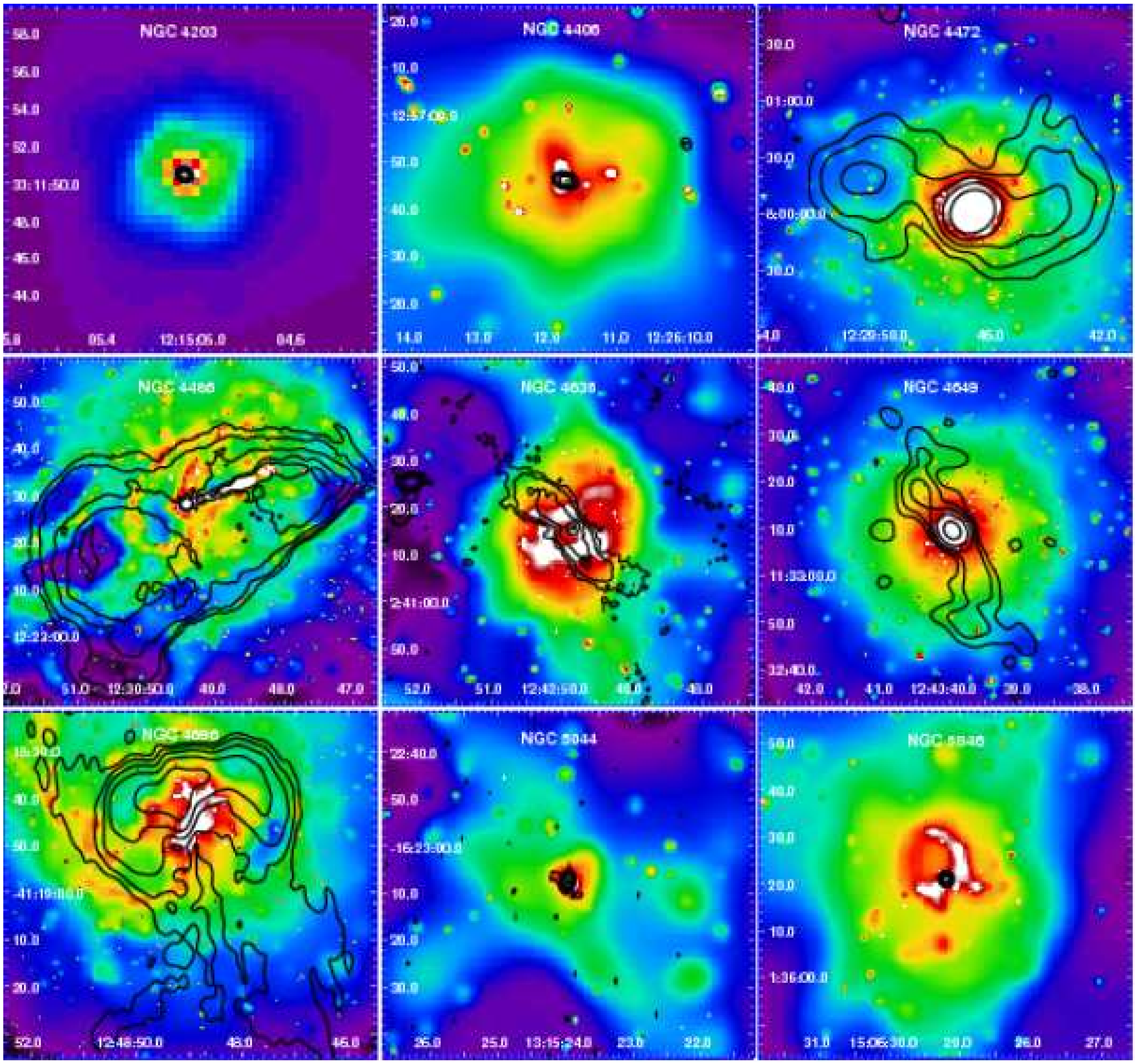

**Figure 2.** (cont.) From top left to bottom right: NGC 4203, NGC 4406, NGC 4472, NGC4486, NGC 4636, NGC 4649, NGC 4969, NGC 5044 and NGC 5846.

### 5.4 NGC 507

NGC 507 is the brightest member of a group of galaxies that is part of the Pisces Cluster. Our radio map has comparatively poor spatial resolution but show that the source is highly extended with two bright lobes in a roughly east-west configuration. *ROSAT* X-ray observations showed NGC 507 to have an extended, bright X-ray halo with a luminosity comparable to that of poor clusters (Kriss et al. 1983; Kim & Fabbiano 1995). The *Chandra* data show some disturbance at the centre of the cluster with indications of a shell of enhanced emission around the eastern radio lobe (Kraft et al. 2004). However, any signs of interaction are less clear around the western lobe, though the secondary western, X-ray bright lump may have been uplifted by the action of the AGN (Forman et al. 2001).

### 5.5 NGC 533

NGC 533 is the dominant galaxy of a group of the same name. Our 4.9 GHz VLA radio data show that the radio emission is dominated by a central point source, although some extension to the west and southwest is detected at modest significance. The X-ray peak is coincident with the central radio source (see Sun 2009; Gastaldello et al. 2007; Piffaretti et al. 2005). On smaller scales, two crescent shaped depressions in the X-ray emission are observed, either side of the peak, with a roughly northeast-southwest orientation (see also Fig. 4). The resolution of the current radio data is insufficient to determine unambiguously whether these features are the result of AGN interaction. The cavities are therefore classified as ‘possible’ rather than ‘definite’. The larger scale X-ray emission also exhibits northeast–southwest elongation, with a bay-like feature to the southwest. Low-frequency radio observations would be required to investigate whether this bay is associated with a past generation of AGN activity.

### 5.6 NGC 708

NGC 708 is the brightest galaxy of the Abell 262 cluster and hosts the radio source B2 0149+35. The VLA data reveal a central point source and two lobes in an east-west configuration. The X-ray emission from the cluster is described by Blanton et al. (2004). A

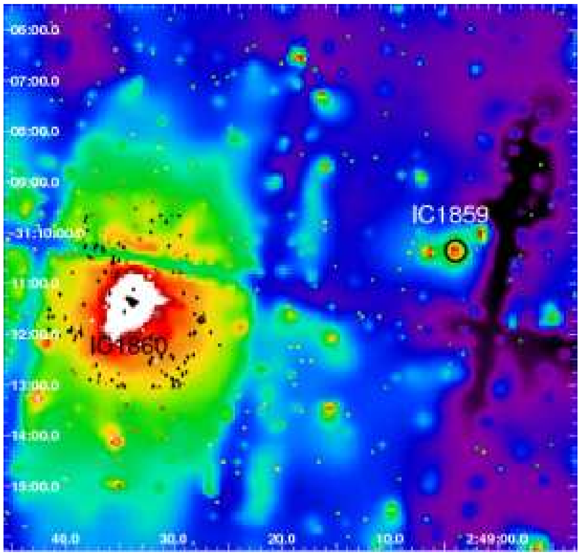

**Figure 3.** The adaptively smoothed *XMM-Newton* X-ray emission surrounding IC 1860 using the same colour scheme as Fig. 2, showing the location of IC 1859 to the west. The radio contours from the observation of IC 1860 are overlaid. The dominant galaxy, at least according to the X-ray emission, appears to be IC 1860.

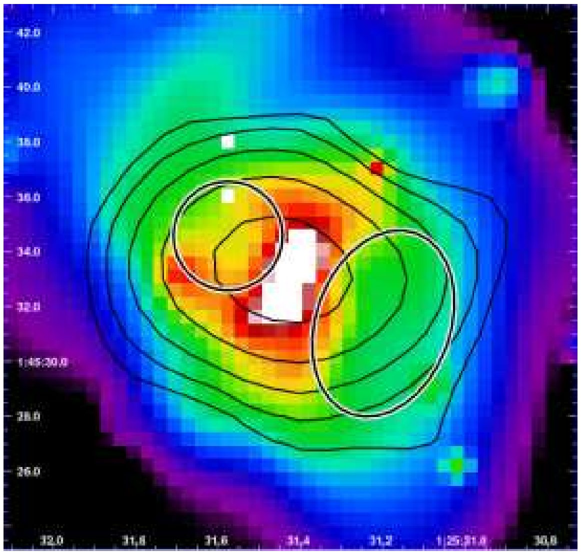

**Figure 4.** Adaptively smoothed X-ray image of NGC 533 using the same colour scheme as Fig. 2 with the radio contours overlaid in black, and the two depressions in the X-ray emission mentioned in the text highlighted. Their radii/semi-major axes are $0.88$ for the north-eastern and $0.92 \times 1.31\,\mathrm{kpc}$ for south-western cavities.

combined study of low frequency radio and X-ray data is presented by Clarke et al. (2009), showing the interaction of the radio source with its surroundings.

### 5.7 NGC 1399

NGC 1399 is the dominant galaxy in the Fornax Cluster (Abell S0373). The radio and X-ray properties are described by Shurkin et al. (2008). The radio source exhibits a nucleus with two tightly collimated jets that feed into more extended radio lobes. The X-ray emission is peaked on the central AGN. Regions of enhanced X-ray emission are observed just beyond the radio lobes (Shurkin et al. 2008).

### 5.8 NGC 1404

NGC 1404 is a member of the Fornax Cluster, in the process of falling towards the centre (NGC 1399, Machacek et al. 2005). Our VLA A-configuration data show a faint central point source. The radio source is also clearly detected in the NVSS catalogue. The X-ray emission map is fairly symmetric and also does not show any features that would indicate significant interaction between the central AGN and surrounding X-ray gas (Machacek et al. 2005).

### 5.9 NGC 1550

NGC 1550, also known as NGC 1551, is the dominant galaxy of the NGC 1550 group. The source exhibits an unusual radio morphology with two peaks: one approximately centered on NGC 1550 and the other offset $\sim 45$ arcsec to the west. The group is unusually X-ray luminous for its temperature and velocity dispersion. The X-ray emission is elliptical, with the semi major axis in the same direction as the axis of the radio source (Sun et al. 2003). A filament of X-ray emission traces the eastern radio lobe, wrapping around the southern part. The western radio peak appears uncorrelated with the X-ray emission. It is possible that the western radio peak is actually due to a background source, although the NASA[10] Extragalactic Database[11] lists no source at this position. It is also possible that radio emission from NGC 1550 has expanded in the surrounding ICM in a highly asymmetric way to create the western peak.

### 5.10 NGC 4203

NGC 4203 is an S0 galaxy hosting a low-luminosity low-ionisation nuclear emission region (LINER) type AGN (LLAGN) (Iyomoto et al. 1998). Point like radio emission is detected in our $4.9\,\mathrm{GHz}$ VLA data. The *Chandra* observation shows an X-ray structure similar to IC 310. There is very little diffuse emission, with most of the X-rays coming from a point source coincident with the radio emission.

### 5.11 NGC 4406

Also known as M 86, NGC 4406 is the dominant member of a small group falling at high velocity towards the centre of the Virgo cluster (NGC 4486/M 87). Our $4.9\,\mathrm{GHz}$ VLA radio data reveal a central point source. *XMM-Newton* and *Chandra* observations of the galaxy are discussed by Finoguenov et al. (2004) and Randall et al. (2008), respectively. Our Chandra image shows only the core of the X-ray emitting gas. There are no clear X-ray features indicating an interaction between the radio and X-ray plasmas.

---

[10] National Aeronautics and Space Administration

[11] NASA/IPAC Extragalactic Database (NED) is operated by the Jet Propulsion Laboratory, California Institute of Technology, under contract with the National Aeronautics and Space Administration.

### 5.12 NGC 4472

Also known as M 49, this Seyfert 2 galaxy is the optically brightest elliptical in the Virgo cluster. It is also the dominant member of a small group. The central radio source has a typical FRI structure but is unusually weak (Ekers & Kotanyi 1978). We present the data from the VLA in C configuration. As noted in Section 3, the data from the A configuration has a $(u, v)$ coverage such that the large scale emission is not detected, and hence we present the C configuration data. The VLA data is a comparatively short observation, but the morphology matches that seen in the FIRST[12] survey observation, presented in Biller et al. (2004); Allen et al. (2006). There are cavities in the X-ray emitting gas corresponding to the radio lobes (Biller et al. 2004).

### 5.13 NGC 4486

NGC 4486, also known as M 87 (Virgo A), is the dominant galaxy at the centre of the Virgo Cluster. It hosts the well studied radio-bright AGN 3C 274. A bright radio jet is also clearly visible in the VLA images, although the contours plotted have been chosen to highlight the diffuse emission surrounding the core. The jet is also clearly seen at X-ray wavelengths. The large scale structure of the ICM and radio emission in NGC 4486 is complex (see e.g. Hines et al. 1989; Owen et al. 2000; Young et al. 2002; Di Matteo et al. 2003; Forman et al. 2005; Kovalev et al. 2007; Forman et al. 2007).

### 5.14 NGC 4636

NGC 4636 (also known as NGC 4624) lies in the southern regions of the Virgo cluster, some $2.6$ Mpc from NGC 4486. The radio data show a central core and two clear lobes. The X-ray morphology is highly disturbed and suggests that a much larger AGN outburst has occurred in the past (see also Jones et al. (2002); O'Sullivan et al. (2005); Baldi et al. (2009)).

### 5.15 NGC 4649

NGC 4649, also known as M 60 is located in a group at the eastern edge of the Virgo Cluster. Recent detailed analyses of the radio and X-ray properties of this source can be found in Randall et al. (2004); Shurkin et al. (2008); Humphrey et al. (2008). In the deeper Chandra data presented here, faint fingers of X-ray emission are observed to surround the radio emission, indicating a channel carved by the AGN jet. Cavities are seen in the X-ray gas at positions correlated with the radio emission from the AGN, confirming the results of Shurkin et al. (2008). These appear as "wedges" pointing to the surface brightness peak in Fig. 2. To clarify the location of the cavities we subtract a spherical profile (beta model) which is fitted to the adaptively smoothed image. The subtracted image is shown in Fig. 5.

### 5.16 NGC 4696

NGC 4696 is the dominant galaxy of the Centaurus Cluster (Abell 3526) and hosts the radio source PKS 1245-41. The radio emission has two clear lobes. High frequency radio emission shows that the jets initially travel east-west before both turning south (Taylor et al. 2002). The interaction of the radio source with the surrounding intra-cluster medium is strikingly clear and is discussed in detail by Sanders & Fabian (2002); Fabian et al. (2005); Taylor et al. (2006).

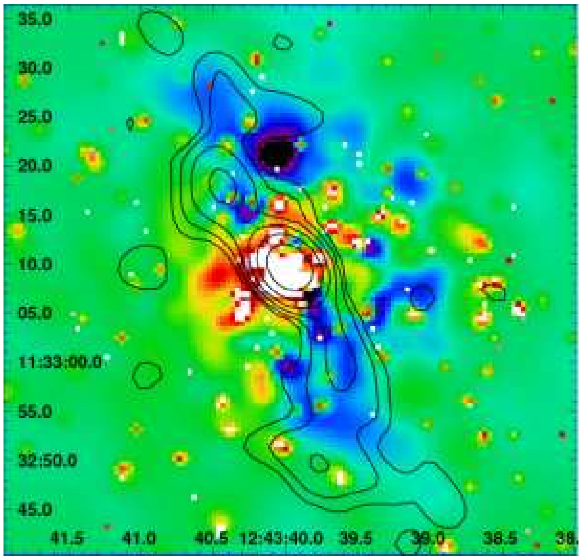

**Figure 5.** The central regions of NGC 4649 where a spherical (beta) model subtracted from the adaptively smoothed image. The colour scheme is the same as in Fig. 2. The depressions associated with the radio emission (black contours) are clearly visible to the north and south of the core.

### 5.17 NGC 5044

NGC 5044 is the central member of a rich group (Rickes et al. 2004)). Our VLA A-configuration data detect a central point radio source. The X-ray emission at the centre of this group is disturbed (Buote et al. 2003a,b). Gastaldello et al. (2009) cite evidence for a pair of bubbles, one north and one south of the X-ray core. Although there is no high frequency radio emission associated with them, H$\alpha$ and [ N II ] emission does appear to be correlated with depressions in the X-ray gas (Gastaldello et al. 2009; Caon et al. 2000). More recent GMRT[13] observation show that the southern cavity is filled by radio plasma emitting at $610$ and $235$ MHz radio emission (David et al. 2009).

### 5.18 NGC 5846

NGC 5846 is one of a dominant galaxy pair (with NGC 5850) of the NGC 5846 group. Our VLA A-configuration data detect a central point radio source. The morphology of the X-ray emission is highly suggestive of an AGN interaction, with a clear circular cavity to the north-east of the core (Trinchieri & Goudfrooij 2002). There is also a wedge to the south west that is fainter than might otherwise be expected. Since no radio emission is associated with the X-ray cavities, here we conservatively classify them as 'possible' rather than 'definite'. Deeper, low frequency radio observations are required.

---

[12] Faint Images of the Radio Sky at Twenty Centimetres, http://sundog.stsci.edu/ (Becker et al. 1995)

[13] Giant Metrewave Radio Telescope

## 6 POPULATION STUDY

### 6.1 Prevalence of Radio Activity

Our sample contains the X-ray brightest, early-type (elliptical and S0) galaxies in the local universe. The sample is drawn from a parent catalogue of optically-selected, optical magnitude-limited galaxies that is itself approximately 90 per cent complete. Using deep VLA observations we have investigated the radio fluxes and morphologies of our galaxies. Only one of the 18 galaxies in the sample is not detected at radio wavelengths (NGC 499). Thus, 94 per cent of our sample have some level of radio activity at their cores.

The one galaxy for which no central radio source is detected, NGC 499, is an X-ray bright lenticular (E/S0) galaxy. The upper limits on the radio emission from this galaxy are stringent. Compared to all other galaxies, NGC 499 is very deficient in its $1.5$ GHz radio luminosity.

Of the 17/18 galaxies with detected radio emission, 10 (55 per cent) have extended radio lobes. We note that most of our observations are only at one frequency, and future observations, especially at low frequencies, may detect extended features in some sources which so far only exhibit a point source. In all cases (apart from IC 310) where the radio morphology is clearly extended, there are features in the X-ray emission which correlate with the radio lobes, although in one case they are faint. The converse is not quite true. In total there are 12 galaxies (67 per cent) which have disturbed X-ray morphologies, which in some cases are clearly bubble-like. These 12 include all nine which have extended radio emission (excluding IC 310). The other three (NGC 533, NGC 5044 and NGC 5846) have bubble-like features in the X-ray emission, but show no clear link to the high frequency radio morphology.

For the radio point sources, deeper and lower frequency observations with the Long Wavelength Array (LWA, Ellingson et al. 2009) or Low Frequency Array (LOFAR, de Vos et al. 2009; both LOFAR and the LWA are currently under construction.) would be useful in searching for past episodes of activity from the central AGN.

Unfortunately 4/18 of our galaxies are observed at $4.9$ GHz[14]. We therefore note that the observations of these galaxies are therefore slightly biased against detecting extended radio emission. Hence, the number of galaxies which have extended radio emission could be a lower limit on the true number.

Only two of the eighteen galaxies in our sample, IC 310 and NGC 4203, host strong X-ray emitting AGN. However, the inclusion of these two galaxies does not affect our results or conclusions significantly.

### 6.2 The link between cool cores and radio activity

**Table 4.** BCES fits to $T_{\rm cool}$ vs $L_{\rm R}$

| Method | Slope | Intercept | Bootstrap Slope |
|---|---|---|---|
| BCES(Y—X) | $-0.138 \pm 0.0515$ | $3.96 \pm 1.93$ | $-0.146 \pm 0.0631$ |
| BCES(X—Y) | $-0.383 \pm 0.147$ | $13.3 \pm 5.56$ | $-0.457 \pm 0.926$ |
| BCES Bisector | $-0.257 \pm 0.0714$ | $8.47 \pm 2.66$ | $-0.275 \pm 0.123$ |
| BCES Orthogonal | $-0.142 \pm 0.0538$ | $4.14 \pm 2.07$ | $-0.151 \pm 0.0664$ |

The slopes from the BCES estimator are also shown in Fig. 6.

Recent observations of the action of AGN at the centres of groups and clusters have alluded to a feedback process between the AGN and the surrounding gas (see e.g. Churazov et al. 2002; Allen et al. 2006; McNamara & Nulsen 2007). The cooling of the X-ray emitting gas provides the fuel for the AGN, whose output is therefore regulated by the amount of gas cooling. However, the output of the AGN prevents the gas from cooling as rapidly as it otherwise would. Estimates of the energy injected by the AGN into the central regions of the clusters and galaxies appears to match that required to prevent (excessive) cooling (e.g. Bîrzan et al. 2004; Dunn & Fabian 2006; Rafferty et al. 2006). However, the details of the coupling of the injected energy to the intracluster medium or galactic halo are not fully understood. Attempts at modelling this self-regulated feedback have made some progress over recent years (e.g. Vernaleo & Reynolds 2006; Brüggen et al. 2009), but as yet there is no observational evidence of the coupling mechanisms. Hence, this picture of feedback is conceptually attractive, although a number of details remain unclear.

To test this scenario, we calculate the mean mass-weighted cooling times within $1\,{\rm kpc}$ for all the galaxies and compare them to $L_{\rm R}$, the monochromatic radio luminosity (see Fig. 6). Here, $L_{\rm R} = \nu_{\rm R} L_{\nu_{\rm R}}$ where $\nu_{\rm R}$ and $L_{\nu_{\rm R}}$ are the observing frequency and monochromatic radio luminosity as shown in Table 5. The cooling times indicate how rapidly the gas is cooling onto the SMBH, and hence give a rough measure of the fuelling rate of the AGN. The radio luminosity, as we include the large scale emission from the radio lobes, gives a crude measure of the mechanical output of the AGN from the relativistic jets. For more precise calculations with a smaller sample, see Allen et al. (2006).

In many of the X-ray observations of the galaxies in the sample a central point source was identified and removed. This creates a minimum radius for which our annular deprojection can obtain values for the cooling time. For these systems, to estimate the cooling time we fit simple power laws to the density and cooling time profiles and extrapolate these inwards to obtain appropriate values for the missing inner annular region. Monte Carlo simulations are used to estimate the final uncertainties in the results.

Setting aside the two galaxies for which the X-ray emission is dominated by nuclear sources (IC 310 and NGC 4203) we observe (see Fig. 6) a slight anti-correlation between the radio luminosity and the mass-weighted cooling time, with a slope of $-0.14$. The BCES Akritas & Bershady (1996) slope estimators are shown in Table 4, and take into account uncertainties in both parameters and the possible presence of intrinsic scatter. Although the sample is small and the scatter is large, we do see indication of a link between the central cooling times and the radio luminosity which is intriguing.

Our findings are consistent with the results of Allen et al. (2006) and lend further support to the idea that the X-ray gas fuels the central AGN in these systems.

Even in this comparatively small sample, the link between extended radio emission and features in the X-ray gas is not totally clear. Although all sources which have extended radio emission have features in the X-ray gas, the converse is not true. In studying the effect of AGN on their surroundings, using *only* the X-ray morphology could give misleading results. The selection involved in finding AGN-inflated cavities are not presently well understood

---

[14] The VLA archive was searched to find the radio observations which showed the most detail for these galaxies, with the aim to find $1.4$ GHz observations. $4.9$ GHz observations were only used when no suitable $1.4$ GHz observations were found.

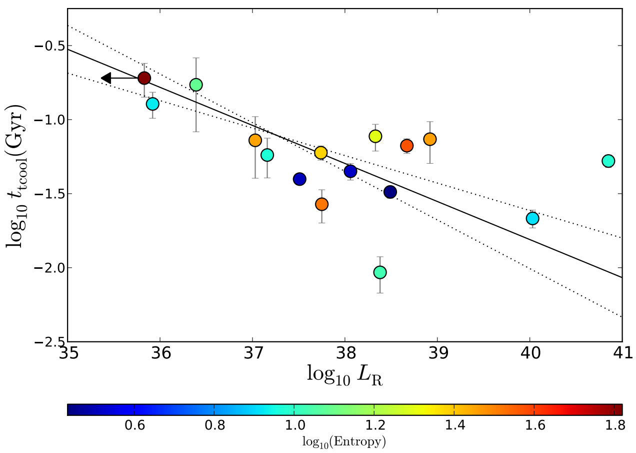

**Figure 6.** The mass-weighted cooling time within 1 kpc against the $L_{\nu_{\rm R}}$ for all galaxies except IC 310 and NGC 4203. The best fit lines shown are the BCES Bisector (solid) along with the errors on the Bisector (dotted) are shown. The colour scale shows the mass-weighted central entropy within 1 kpc for the galaxies.

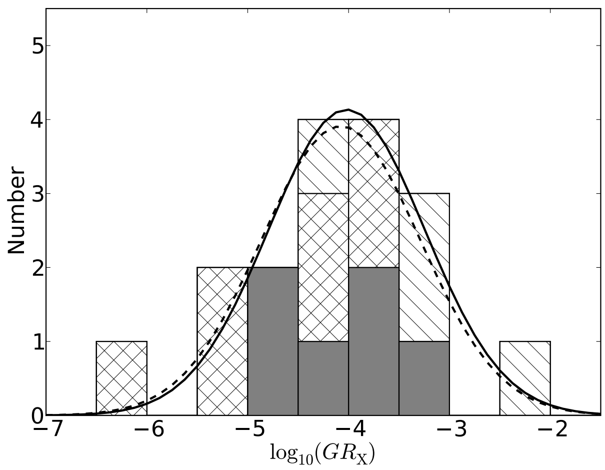

**Figure 7.** The distribution of $\log(\mathcal{GR}_X)$ for the sample of 17 galaxies with detected radio emission. The hashed bars are the group dominant- , the cross-hashed are the cluster dominant- and the solid bars are the non-dominant galaxies. The two fitted curves are for a least-squares (dashed) and a downhill simplex (solid) Gaussian model fit to the total distribution. IC 310 and NGC 4203 are included in this plot.

(Nulsen et al. 2007; Birzan et al. 2009). The fraction of galaxies showing AGN inflated cavities in this sample is around twice what Nulsen et al. (2007) report. The high level of core radio detections in the sample presented here indicate that, *(a)* the fraction of AGN currently injecting mechanical energy into their surrounding could be much higher than previously thought, and *(b)* the criteria for an AGN to be “active” need to be quantified.

The AGN in the elliptical galaxies with detected cavities in Nulsen et al. (2007) appear to be injecting more energy than required to offset the cooling of the X-ray gas. This may result if the cavities for an average elliptical are very difficult to detect, and so only exceptional (overpowered) outbursts are (usually) observed. For lower mass systems (groups and ellipticals), the overall level of (mechanical) energy injection into their surrounding environments remains incompletely understood.

### 6.3 Radio-to-X-ray flux ratios

We have determined integrated radio-to-X-ray flux ratios for the galaxies. The measured quantity, $\mathcal{GR}_{\rm X}$, follows the radio-to-X-ray loudness parameter for nuclear AGN emission, $\mathcal{R}_{\rm X}$, determined by Terashima & Wilson (2003). We write

$$\mathcal{GR}_{\rm X} = \nu_{\rm R} L_{\nu_{\rm R}} / L_{\rm X}. \qquad (1)$$

where $L_{\rm X}$ is the $0.1 - 2.4\,{\rm keV}$ band X-ray luminosity. Terashima & Wilson (2003) note that the boundary between radio-loud and radio-quiet nuclear sources occurs at $\log_{10}(\mathcal{R}_{\rm X}) = -4.5$.

The distribution of $\log_{10}(\mathcal{GR}_{\rm X})$ is shown in Fig. 7, with the data detailed in Table 5. As can be seen from Fig. 7, there is a large spread in $\log(\mathcal{GR}_X)$. Also shown are the results of fitting a Gaussian model to the distribution: the peak of the Gaussian lies at $\log_{10}(\mathcal{GR}_{\rm X}) = -4.02\ (-4.08)$ with a variance of $0.78\ (0.79)$ for a downhill simplex (least squares) fit.

We have also calculated $\mathcal{GR}_{\rm X,\,NVSS}$ values based on the radio flux densities determined from the NVSS Survey (Condon et al. 1998). We show the monochromatic radio luminosities from the NVSS, $L_{\rm R,\,NVSS}$, along with the $\mathcal{GR}_{\rm X,\,NVSS}$ in Table 5. The NVSS flux densities were all measured at $1.4\,{\rm GHz}$ using a more compact configuration of the VLA. More faint emission is included at the price of the lower spatial resolution. There are some differences between the values of $\mathcal{GR}_{\rm X}$ calculated from the high spatial resolution VLA observations and those from the NVSS. However, all but one (IC 310) differ by less than a factor of two. All galaxies in our sample have NVSS detections. See Section 7 for more on the NVSS properties.

Our sample contains four dominant cluster galaxies (NGC 708, NGC 1399, NGC 4486, NGC 4696), seven dominant group galaxies (IC 1860, NGC 507, NGC 533, NGC 1550, NGC 4406, NGC 4649, NGC 5044) and seven galaxies (IC 310, NGC 499, NGC 1404, NGC 4203, NGC 4472, NGC 4636, NGC 5846) that are $not$ the dominant galaxy of a group or cluster. We see no significant difference in the $\mathcal{GR}_{\rm X}$ values for dominant and non-dominant galaxies.

### 6.4 Prevalence of Radio-Loud AGN

There is a perception that the fraction of AGN in the general population of galaxies is small, even though SMBH are present in most moderately sized galaxies. Part of this perception is historical: early studies only found AGN fractions of a few per cent (Dressler et al. 1985; Huchra & Burg 1992). However, as the data have improved, this fraction has increased (Carter et al. 2001; Miller et al. 2003; Santra et al. 2007) with nuclear activity being found in galaxies that would not, classically, have been classed as AGN. For example, in the Palomar sample of nearby bright galaxies (magnitude limited), Nagar et al. (2005) and Filho et al. (2006) used high resolution radio imaging to show that at least a quarter of galaxies, and probably more, are AGN. However, many of these AGN are low luminosity. In another study, a combined optical and X-ray study of Elliptical galaxies in the Virgo Cluster find X-ray signatures of AGN in the cores of 49-87 per cent target galaxies with stellar masses $> 10^{10} M_{\odot}$ (Gallo et al. 2008). At lower galaxy masses the fraction falls to 3-44 per cent. This decline in the AGN fraction with decreasing galaxy mass has been seen at the cluster and group level by Best et al. (2005).

**Table 5.** Radio Loudness

| Source | Type | Frequency (GHz) | $L_{\rm X}$ (erg s$^{-1}$) | $S_{\nu{\rm R}}$ (erg s$^{-1}$ Hz$^{-1}$) | $L_{\rm R}$ (erg s$^{-1}$) | $\mathcal{GR}_X$ | $L_{\rm R,\,NVSS}$ (erg s$^{-1}$) | $\mathcal{GR}_{\rm X,\,NVSS}$ |
|---|---|---|---|---|---|---|---|---|
| IC 1860 | P | 1.365 | $5.89 \times 10^{42}$ | $1.39 \times 10^{-25}$ | $2.12 \times 10^{39}$ | $3.60 \times 10^{-5}$ | $2.86 \times 10^{38}$ | $4.86 \times 10^{-5}$ |
| NGC 499 | P | 1.365 | $2.24 \times 10^{42}$ | - | - | - | - | - |
| NGC 507 | E | 1.525 | $5.75 \times 10^{42}$ | $8.74 \times 10^{-25}$ | $8.27 \times 10^{38}$ | $1.44 \times 10^{-4}$ | $5.36 \times 10^{38}$ | $9.31 \times 10^{-5}$ |
| NGC 533 | P | 4.885 | $1.95 \times 10^{42}$ | $8.91 \times 10^{-26}$ | $2.42 \times 10^{38}$ | $1.24 \times 10^{-4}$ | $2.23 \times 10^{38}$ | $1.14 \times 10^{-4}$ |
| NGC 708 | E | 1.365 | $1.23 \times 10^{43}$ | $8.25 \times 10^{-25}$ | $4.72 \times 10^{38}$ | $3.83 \times 10^{-5}$ | $3.85 \times 10^{38}$ | $3.13 \times 10^{-5}$ |
| NGC 1399 | E | 1.465 | $4.90 \times 10^{41}$ | $4.63 \times 10^{-24}$ | $3.06 \times 10^{38}$ | $6.25 \times 10^{-4}$ | $1.31 \times 10^{38}$ | $2.68 \times 10^{-4}$ |
| NGC 1404 | P | 1.365 | $1.78 \times 10^{41}$ | - | - | - | $2.46 \times 10^{36}$ | $1.38 \times 10^{-5}$ |
| NGC 1550 | E | 1.365 | $7.24 \times 10^{42}$ | $1.27 \times 10^{-25}$ | $5.07 \times 10^{37}$ | $7.73 \times 10^{-6}$ | $7.51 \times 10^{37}$ | $1.04 \times 10^{-5}$ |
| NGC 4203 | P | 4.885 | $1.74 \times 10^{41}$ | $1.80 \times 10^{-25}$ | $3.18 \times 10^{37}$ | $1.83 \times 10^{-4}$ | $3.09 \times 10^{36}$ | $1.78 \times 10^{-5}$ |
| NGC 4406 | P | 4.885 | $1.29 \times 10^{42}$ | $4.91 \times 10^{-27}$ | $8.35 \times 10^{35}$ | $6.48 \times 10^{-7}$ | - | - |
| NGC 4472 | E | 1.489 | $3.09 \times 10^{41}$ | $2.23 \times 10^{-24}$ | $1.16 \times 10^{38}$ | $3.74 \times 10^{-4}$ | $1.07 \times 10^{38}$ | $3.47 \times 10^{-4}$ |
| NGC 4486 | E | 1.435 | $1.02 \times 10^{43}$ | $8.73 \times 10^{-22}$ | $7.01 \times 10^{40}$ | $6.85 \times 10^{-3}$ | $6.75 \times 10^{40}$ | $6.60 \times 10^{-3}$ |
| NGC 4636 | E | 1.425 | $4.47 \times 10^{41}$ | $6.45 \times 10^{-25}$ | $3.20 \times 10^{37}$ | $7.16 \times 10^{-5}$ | $3.79 \times 10^{37}$ | $8.49 \times 10^{-5}$ |
| NGC 4649 | E | 1.465 | $2.19 \times 10^{41}$ | $2.82 \times 10^{-25}$ | $1.44 \times 10^{37}$ | $6.58 \times 10^{-5}$ | $1.42 \times 10^{37}$ | $6.48 \times 10^{-5}$ |
| NGC 4696 | E | 1.565 | $1.95 \times 10^{43}$ | $3.64 \times 10^{-23}$ | $1.07 \times 10^{40}$ | $5.50 \times 10^{-4}$ | - | - |
| NGC 5044 | P | 1.465 | $6.31 \times 10^{42}$ | $2.99 \times 10^{-25}$ | $5.49 \times 10^{37}$ | $8.70 \times 10^{-6}$ | $6.09 \times 10^{37}$ | $9.65 \times 10^{-6}$ |
| NGC 5846 | P | 1.465 | $5.13 \times 10^{41}$ | $1.02 \times 10^{-25}$ | $1.08 \times 10^{37}$ | $2.10 \times 10^{-5}$ | $2.12 \times 10^{37}$ | $4.13 \times 10^{-5}$ |
| IC 310 | E | 1.465 | $3.98 \times 10^{42}$ | $1.50 \times 10^{-24}$ | $1.21 \times 10^{39}$ | $3.05 \times 10^{-4}$ | $1.30 \times 10^{39}$ | $3.26 \times 10^{-4}$ |
| NGC 4203 | P | 1.465 | $1.74 \times 10^{41}$ | $7.86 \times 10^{-26}$ | $4.15 \times 10^{36}$ | $3.10 \times 10^{-4}$ | $3.09 \times 10^{36}$ | $1.78 \times 10^{-5}$ |

The Types show whether the radio morphology is P-point like or E-extended. The $L_{\rm R}$ are calculated at the frequency shown in the table, without any scaling to a common frequency. We also show the $L_{\rm R,\,NVSS}$ calculated from the NVSS, which are all at the same frequency. We separate IC 310 and NGC 4203 which appear to be a different class of source as the other galaxies.

In determining the fraction of radio loud galaxies present in a sample of SDSS galaxies Best et al. (2005) use a limit for radio loudness of $L_{1.4\,{\rm GHz}} > 10^{23}$W Hz$^{-1}$. We converted this limit to a luminosity limit at the frequency of the NVSS catalogue (1.5 GHz). Therefore, any galaxy with $L_{\rm R,\,NVSS} > 1.4 \times 10^{39}$ erg s$^{-1}$ would be classed as radio-loud in Best et al. (2005). In our sample only NGC 4486 is above this limit; however NGC 4696 would also be if it was in the NVSS catalogue, and IC 310 falls directly on the boundary. This gives a radio loud fraction of 11 per cent, (2/18) and 17 per cent (3/18) if including IC 310. We show the distribution of radio luminosity with X-ray luminosity in Fig. 8, along with the threshold value for radio-loudness from Best et al. (2005).

This radio loud fraction is much lower than the *radio detected* fraction in our sample (17/18). Although using a cut-off in the $L_{1.4\,{\rm GHz}}$ ensures selecting AGN radio activity out to large distances, the results from this study shows that it does not include a large number of AGN with low radio luminosities. Of the AGN which are not included when using a radio luminosity cut-off, a significant fraction have extended radio emission, though others are just radio cores. To obtain a clearer picture of the level of radio activity within a sample of galaxies, the radio-to-X-ray flux ratio (Section 6.3) of a galaxy can be used. The two galaxies which are classed as radio loud from the radio luminosity limit both have extended radio lobes. However a further 8 (including IC 310) also have extended radio emission, indicating active mechanical energy injection into their surroundings. Therefore the radio luminosity limit results in an incomplete picture of the level of energy injection into the surroundings of elliptical galaxies.

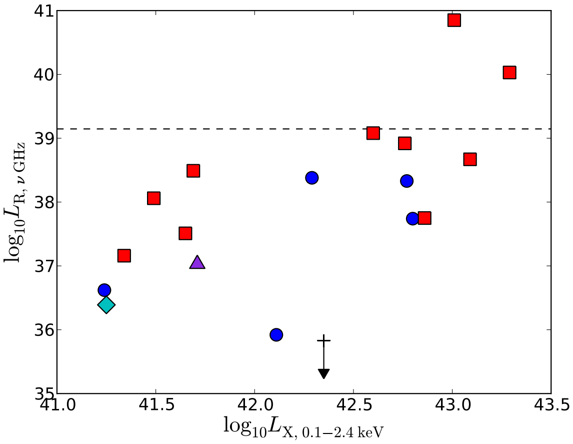

**Figure 8.** The radio luminosity ($L_{\rm R,\nu}$) as a function of the X-ray luminosity ($L_{\rm X,0.1-2.4keV}$) along with a dashed line showing radio loudness cut-off used by Best et al. (2005). The red squares are extended radio sources and the blue circles are radio point sources. The purple triangle is NGC 5846 which although being a point source has clear indications of interactions in the X-ray emission. The cyan diamond is NGC 1404 using NVSS data. The upper limit for NGC 499 is also shown. The limitations of using a cut-off in the $L_{1.4\,{\rm GHz}}$ are clear.

Although our sample selects massive galaxies which are X-ray bright, we are not purposefully selecting AGN host galaxies; central point sources typically account for only a very small fraction of the total X-ray flux. Our results indicate that AGN activity is common in most massive galaxies; massive galaxies being the ones which are more likely to have and be able to retain a halo of X-ray gas.

In a large sample of clusters and groups of galaxies, Best et al. (2007) find that brightest group and cluster galaxies are more likely to host a radio loud AGN than a field galaxy of an equivalent mass. This increased likelihood also extends to galaxies which are close to the cluster centre. Not all of our targets are dominant galaxies. Most are in clusters or groups. The two most radio loud sources in our study are the brightest galaxies of the Virgo and Centaurus Clusters.

### 6.5 Particle Content

Here we follow the analysis in Dunn & Fabian (2004); Dunn et al. (2005) and more recently Croston et al. (2005); De Young (2006); Shurkin et al. (2008) and Croston et al. (2008) in studying the particle content of the radio lobes. Under the assumption that the relativistic radio-emitting plasma is in pressure balance with the X-ray gas, we are able to determine the energy, and hence particle content of the radio plasma.

Measurements of the synchrotron emission from the radio lobes can be used to calculate the energy contained within the relativistic electrons present in the lobes. Fabian et al. (2002) studied the lobes of 3C 84 in the Perseus cluster. Subsequently Dunn & Fabian (2004); Dunn et al. (2005) investigated a larger number of radio sources in galaxy clusters. For a more detailed description of the method see e.g. Dunn & Fabian (2004).

For a continuous synchrotron spectrum with a single spectral index, $\alpha$, between $\nu_1 = 10\,\mathrm{MHz}$ and $\nu_2 = 10\,\mathrm{GHz}$, the energy in relativistic elections is

$$\begin{aligned} E_{\mathrm{e}} &\propto \frac{S_\nu}{\nu} \frac{\nu_2^{0.5+\alpha} - \nu_1^{0.5+\alpha}}{\alpha + 0.5} B^{-3/2}\,\mathrm{erg} \qquad (2)\\ &\approx aB^{-3/2} \qquad (3) \end{aligned}$$

Also taking into account the energy within the magnetic field, the total energy in the lobes is

$$E_{\mathrm{tot}} = kE_{\mathrm{e}} + Vf\frac{B^2}{8\pi}, \qquad (4)$$

where $k$ accounts for any other particles present in the lobe which are not accounted for by the simplistic model spectrum. $V = \frac{4}{3}\pi R_{\mathrm{l}} R_{\mathrm{w}}^2$ is the volume of the bubble, where $R_{\mathrm{l}}$ and $R_{\mathrm{w}}$ are the bubble radii along and perpendicular to the jet axis respectively. $f$ is the volume filling fraction of the relativistic plasma.

The magnetic field present inside the bubble is estimated by comparing the synchrotron cooling time of the plasma to the age of the lobe. The latter can be estimated from the sound-speed expansion timescale[15]. No strong shocks are seen in the X-ray gas, so sound speed expansion timescale gives a lower limit on the age of the bubbles, and hence an upper limit on the magnetic field.

We obtain upper limits on the ratio $k/f$,

$$\frac{k}{f} \leqslant \left(P_{\mathrm{th}} - \frac{B^2}{8\pi}\right)\frac{3V}{a}B^{3/2} \qquad (5)$$

for all galaxies with extended radio emission, where the $3V$ arises from the energy density of the relativistic particles. If $k/f = 1$, i.e. $\log_{10}(k/f) = 0$, then the lobe is filled with a purely electron-positron plasma with emission only in the range $10\,\mathrm{MHz}$ to $10\,\mathrm{GHz}$. Under the assumption $f \sim 1$, then if $k/f > 1$, $k > 1$, which implies that there are “extra” particles required for the lobe to be in pressure balance with its surroundings. These could be thermal protons, mixed into the relativistic plasma as the jet travels out from the AGN, or they could be electrons which radiate out of the assumed region. Since we assume a simple power-law slope for the spectral index, any large deviation at low (and hence unobserved) radio frequencies will also change the calculated $k/f$. We have also determined the value of $k/f$ if the sources were to be in equipartition. However in none of the radio bubbles does equipartition between the relativistic particles and the magnetic field lead to pressure balance between the radio and X-ray plasmas.

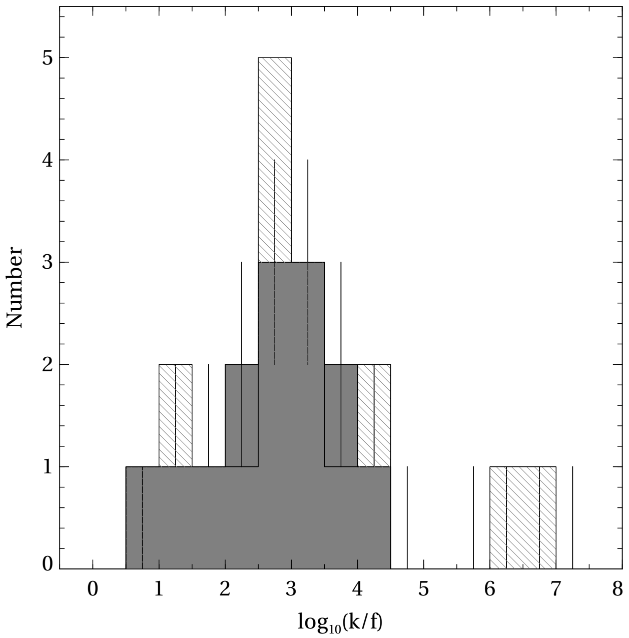

**Figure 9.** The distribution of the upper limits on $k/f$ for the 16 galaxies which have extended radio emission. We show both a standard binning (hashed) and a Monte-Carlo routine which was used to account for the large uncertainties of the $k/f$ values (solid). The errorbars are from the Monte-Carlo routine and are for the solid bars.

As can be seen from Table 6, our sample exhibits a large range of $k/f$ upper limits. The distribution of values is also shown in Fig. 9. (We use a Monte Carlo algorithm to estimate the uncertainties in the upper limits). The distribution of $k/f$ is broad, in agreement with the conclusions of e.g. Dunn et al. (2005); Bîrzan et al. (2007).

#### 6.5.1 *Low Frequency Radio Spectrum*

The value of $k/f$ is expected to increase as a plasma ages with synchrotron losses, causing the average energy of the particles to drop. Electrons with low energies will emit at frequencies below the observed energy range and act as “extra particles” in the model. Since bubbles will only appear ‘young’ for a short time, most will be seen when $k/f$ is large. Eventually the radio emission will drop below detection limits, leading to an upper limit to the values of $k/f$ estimated from GHz radio data. There is a suggestion from Fig. 9, that the distribution peaks at around $10^3$, but with asymmetric tails either side.

We have investigated whether, by modifying the spectrum to include additional low frequency radio emission from low energy particles (extending $\nu_1 = \nu_{\mathrm{min}} < 10\,\mathrm{MHz}$), it is possible to achieve $k/f$ equal to one. The minimum possible radio frequency is the cyclotron frequency as estimated from the magnetic field estimates. For around half of the bubbles $k/f = 1$ is achieved before the frequency limit is reached. The bubbles for which $k/f = 1$ is not achievable are those which have the largest $k/f$ values to start with.

In some of the galaxies in our sample, there is no extended $1.4\,\mathrm{GHz}$ radio emission, even when there are features in the X-

---

[15] Since the radio lobes of interest are still attached to the active radio jets, this is the most sensible, easy to calculate, timescale.

**Table 6.** $k/f$ Results

| Galaxy | Lobe | $R_\mathrm{l}$ (kpc) | $R_\mathrm{w}$ (kpc) | $R_\mathrm{Dist}$ (kpc) | $S$ (Jy) | $\alpha$ | $\log(B)$ | $\log(k/f_\mathrm{eqptn})$ | $\log(k/f_\mathrm{sound})$ | $\log(\nu_\mathrm{min})$ | $\log(k/f_{\nu_\mathrm{min}})$ |
|---|---|---|---|---|---|---|---|---|---|---|---|
| NGC507 | E | 10.70 | 15.20 | 14.90 | 0.027 | $-1.40 \pm 0.20$ | $-5.09 \pm 0.02$ | $2.83 \pm 0.34$ | $2.77 \pm 0.34$ | $4.04 \pm 0.95$ | $-0.00 \pm 0.02$ |
| NGC507 | W | 11.00 | 14.30 | 12.20 | 0.048 | $-1.40 \pm 0.20$ | $-5.10 \pm 0.02$ | $2.54 \pm 0.35$ | $2.47 \pm 0.34$ | $4.37 \pm 0.87$ | $-0.00 \pm 0.02$ |
| NGC708 | E | 4.93 | 2.72 | 5.78 | 0.014 | $-0.60 \pm 0.20$ | $-4.86 \pm 0.03$ | $3.52 \pm 0.17$ | $3.34 \pm 0.16$ | $1.58 \pm 0.03$ | $2.68 \pm 0.78$ |
| NGC708 | W | 4.75 | 2.82 | 4.75 | 0.017 | $-0.60 \pm 0.20$ | $-4.85 \pm 0.03$ | $3.44 \pm 0.18$ | $3.28 \pm 0.18$ | $1.59 \pm 0.03$ | $2.61 \pm 0.78$ |
| NGC1399 | N | 2.88 | 1.94 | 8.39 | 0.11 | $-0.90 \pm 0.10$ | $-4.73 \pm 0.03$ | $2.56 \pm 0.17$ | $2.62 \pm 0.17$ | $1.67 \pm 0.03$ | $0.01 \pm 0.02$ |
| NGC1399 | S | 3.96 | 2.50 | 8.42 | 0.13 | $-0.90 \pm 0.10$ | $-4.81 \pm 0.03$ | $2.60 \pm 0.18$ | $2.65 \pm 0.17$ | $1.63 \pm 0.02$ | $0.01 \pm 0.01$ |
| NGC1550 | E | 4.34 | 6.37 | 5.60 | 0.0035 | $-1.00 \pm 0.50$ | $-4.83 \pm 0.03$ | $6.83 \pm 0.58$ | $6.63 \pm 0.57$ | $1.62 \pm 0.03$ | $-0.01 \pm 0.02$ |
| NGC1550 | W | 7.34 | 4.55 | 10.70 | 0.0029 | $-1.00 \pm 0.50$ | $-4.97 \pm 0.03$ | $6.51 \pm 0.57$ | $6.25 \pm 0.57$ | $1.46 \pm 0.03$ | $-0.01 \pm 0.02$ |
| NGC4472 | E | 2.24 | 2.24 | 4.81 | 0.029 | $-0.80 \pm 0.10$ | $-4.68 \pm 0.03$ | $3.65 \pm 0.15$ | $3.70 \pm 0.15$ | $1.72 \pm 0.03$ | $2.08 \pm 0.60$ |
| NGC4472 | W | 3.07 | 1.83 | 2.82 | 0.038 | $-0.80 \pm 0.10$ | $-4.77 \pm 0.03$ | $3.27 \pm 0.14$ | $3.30 \pm 0.14$ | $1.66 \pm 0.02$ | $1.66 \pm 0.61$ |
| NGC4486 | J | 1.46 | 0.91 | 1.49 | 35.8 | $-0.60 \pm 0.20$ | $-4.47 \pm 0.02$ | $1.13 \pm 0.22$ | $0.97 \pm 0.22$ | $1.96 \pm 0.02$ | $0.01 \pm 0.02$ |
| NGC4486 | CJ | 1.29 | 1.29 | 1.48 | 56.5 | $-0.60 \pm 0.20$ | $-4.44 \pm 0.02$ | $1.23 \pm 0.16$ | $1.11 \pm 0.16$ | $1.99 \pm 0.03$ | $0.01 \pm 0.01$ |
| NGC4636 | NE | 0.71 | 0.41 | 0.82 | 0.028 | $-0.60 \pm 0.20$ | $-4.40 \pm 0.02$ | $2.43 \pm 0.18$ | $2.59 \pm 0.18$ | $2.04 \pm 0.02$ | $0.01 \pm 0.02$ |
| NGC4636 | SW | 0.77 | 0.39 | 0.86 | 0.0185 | $-0.60 \pm 0.20$ | $-4.42 \pm 0.01$ | $2.61 \pm 0.16$ | $2.76 \pm 0.16$ | $2.02 \pm 0.01$ | $0.01 \pm 0.02$ |
| NGC4649 | N | 0.51 | 0.49 | 0.84 | 0.0029 | $-0.60 \pm 0.20$ | $-4.25 \pm 0.02$ | $4.13 \pm 0.16$ | $4.26 \pm 0.16$ | $2.17 \pm 0.01$ | $3.64 \pm 0.70$ |
| NGC4649 | S | 0.65 | 0.42 | 1.03 | 0.0019 | $-0.70 \pm 0.20$ | $-4.32 \pm 0.02$ | $3.93 \pm 0.22$ | $4.06 \pm 0.21$ | $2.12 \pm 0.02$ | $3.04 \pm 0.95$ |
| NGC4696 | E | 2.83 | 1.75 | 2.32 | 1.3 | $-0.75 \pm 0.20$ | $-4.72 \pm 0.02$ | $1.53 \pm 0.25$ | $1.40 \pm 0.25$ | $1.68 \pm 0.03$ | $0.01 \pm 0.01$ |
| NGC4696 | W | 2.88 | 1.96 | 3.24 | 0.65 | $-0.75 \pm 0.20$ | $-4.73 \pm 0.02$ | $1.94 \pm 0.24$ | $1.81 \pm 0.24$ | $1.68 \pm 0.03$ | $0.01 \pm 0.01$ |

$R_\mathrm{l}$ and $R_\mathrm{w}$ are the dimensions of the bubbles with $R_\mathrm{dist}$ their separation from the AGN. $k/f_\mathrm{eq^n}$ is the equipartition value of $k/f$ and $k/f_\mathrm{sound}$ is the value as estimated from the sound speed expansion timescale. $\nu_\mathrm{min}$ is the lower cut off to the radio spectrum required for $k/f = 1$ if it can be reached before the cyclotron frequency. $k/f_{\nu_\mathrm{min}}$ is the value of $k/f$ at that frequency. The bubble descriptors are N-North, S-South, E-East, W-West, J-Jet, CJ-Counter Jet. The spectral indices have been taken from the following; NGC 507 (Colla et al. 1975), NGC 708 (Hardcastle et al. 2003), NGC 1399 (Ekers et al. 1989), NGC 4649 (Stanger & Warwick 1986), NGC 4486 (Hines et al. 1989), NGC 4636 (Stanger & Warwick 1986), NGC 4472 (High-resolution X-ray and radio observations of the giant elliptical galaxies NGC 4636 and 4649 Vol), NGC 4696 (Fabian et al. 2005).

ray emission which point towards an interaction (e.g. NGC 5044 and NGC 5846). Studies which have included low frequency radio emission (e.g. Dunn et al. 2005; Bîrzan et al. 2008) obtain $k/f$ values which are larger than the values from GHz radio emission. However, the increase in $k/f$ for ghost bubbles, regardless of the type of radio emission is currently detected from them, is at least in part an effect of not being able to sample the full radio spectrum of the lobes.

As the electrons age, the synchrotron radio flux in the GHz band falls. Therefore more “extra particles” are required for pressure balance, resulting in a higher value calculated for $k/f$ (assuming $f = 1$). However, the aged synchrotron electrons are still present in the lobe and still supporting it, but radiating at much lower frequencies. Therefore a measure of $k/f$ at GHz frequencies does not fully describe the $k/f$ of the complete lobe. Observations with the new low frequency radio telescopes (LOFAR, LWA or the Murchison Widefield Array Lonsdale & MWA Collaboration 2007) will uncover the spectral shape at low frequencies and so allow further investigations into the detected and the presumed cavities.

### *6.5.2 Possible Biases*

In the calculations outlined above, we have used the sound speed timescale to estimate the age of the bubbles, and compared this age to the synchrotron cooling time of the plasma to estimate the magnetic field. These are not the only possibilities available when calculating the $k/f$ for the cavities.

Older cavities have been described by a buoyancy timescale, the time taken to rise buoyantly in the potential well of the galaxy (Churazov et al. 2000). This buoyant rise takes place after the initial expansion, and separates the cavity from the galactic nucleus. In all of the cavities studied here, they are still attached to the nucleus, with on the whole, radio emission also connected to the radio core. The buoyancy timescale is therefore unlikely to be a reasonable description for the age of the cavities.

Another timescale of interest is the time for the intra-galactic medium to refill the displaced volume (McNamara et al. 2000). However, this is also most applicable to older cavities which have detached from the nucleus and risen up, with the IGM flowing around behind the cavity.

No *strong* shocks are seen around the cavities at the centres of nearby clusters of galaxies (e.g. Perseus, A2052), the expansion of these bubbles is not currently highly supersonic. Although fed by a relativistic jet, and hence at some point expand supersonically, on average the sound speed is an appropriate value to calculate the age of the cavities from. We assume that this is also the case in these, in some cases lower-power, cavity systems.

To obtain an estimate on the magnetic field of the relativistic plasma, we compare the synchrotron cooling time to the age of the cavity. Using the observation that GHz radio emission is detected, we conclude that the synchrotron cooling time must be longer than the age of the cavity. However, we are unable to say how much longer; we can only place a lower bound on the synchrotron cooling time, and hence an upper bound on the magnetic field strength. Future low-frequency radio observations will help in determining the spectral shape of the radio emission, and hence improve the estimates on the magnetic field strength, and hence the age of the bubbles.

Improving the age estimates of the bubbles may be possible with increasingly accurate simulations of the behaviour for the evolution of radio lobes in clusters of galaxies. For older bubbles, a combination of the sound speed expansion and the buoyancy rise time may be the best current description for the ages.

## 7 EXTENDED SAMPLE

We have attempted to extend our study to lower X-ray and radio fluxes. Dropping the flux cut to $1 \times 10^{-12}\,\mathrm{erg\,s^{-1}\,cm^{-2}}$ increases the sample from 18 galaxies to 42. Of these 42 galaxies, 25 (60 per cent) have their $L_X$ values determined from follow-up pointed observations (O'Sullivan et al. 2001). In order to limit our study to the most massive elliptical and S0 galaxies, we introduce a luminosity cut along with the flux cut. Limiting the galaxies to those with $L_X > 10^{41.0}\,\mathrm{erg\,s^{-1}}$ ensures we do not select very nearby low mass galaxies.

To determine the radio properties of these galaxies we use the NVSS survey at $1.4\,\mathrm{GHz}$ for the northern hemisphere, and the Sydney University Molonglo Sky Survey (SUMSS, Bock et al. 1999; Mauch et al. 2003) at $843\,\mathrm{MHz}$ for the southern hemisphere. These surveys, albeit at slightly different frequencies, are comparable in terms of their sensitivity and resolution. Using these, we are able to determine whether the galaxy hosts a radio source. We perform a search using a radius of 30 arcsec in NVSS and then a 60 arcsec search for those galaxies where nothing is found. We use the SUMSS postage stamp cutouts to check those galaxies which are out of the NVSS survey area.

Table 7 summarises the radio information from the NVSS and SUMSS for all galaxies in the extended sample. It is clear that this extended sample still has a very high radio detection rate, with 34/42 (81 per cent) galaxies having a radio detection within NVSS/SUMSS. The radio sensitivity of this analysis is much lower than that in the previous sections, using pointed VLA observations. Therefore the total fraction could be significantly higher. In Fig. 10 we show the distribution of galaxies and those which have radio detections in the NVSS and SUMSS.

For the extended sample we are not able to comment on the morphology of the X-ray emission, and only very coarsely on the radio morphology. However, we can use the classifications given to the galaxies in the SIMBAD[16] database, which are noted in Table 7. There are no galaxies with classifications which would indicate that they have radio emission that we have overlooked/missed with the two surveys used. The galaxies which do not have any radio emission are a mixture of field galaxies, as well as those in groups or clusters, but not dominating them.

We investigated whether from the SIMBAD morphological markers we could clearly determine whether the X-ray emission is likely to be dominated by an X-ray bright AGN. However NGC 4472, NGC 4486 and NGC 4636 have markers of either Seyfert 2 galaxies or a LINER type AGN but all have clear and strong diffuse X-ray emission in addition to the AGN emission. Without high spatial resolution X-ray observations of these galaxies we cannot comment on the ratio of the nuclear to the diffuse X-ray emission in these galaxies.

**Table 7.** Extended Sample

| Galaxy | Flux mJy | Survey | Type | Redshift | $L_X$ $\log_{10}$ erg s$^{-1}$ |
|---|---|---|---|---|---|
| IC310$^*$ | 168.1 | N | GiC | 0.0156 | 42.60 |
| IC1860$^*$ | 18.3 | N | GiC | 0.0221 | 42.77 |
| IC2006 | - | N | GiC | 0.0045 | $<41.09^a$ |
| IC4296 | 546.6 | N | rG | 0.0118 | 41.59 |
| IC4765 | 32.4 | S | GiG | 0.0144 | 41.89 |
| NGC57 | - | N | G | 0.0136 | 41.71 |
| NGC410 | 5.8 | N | GiG | 0.0140 | 41.97 |
| NGC499$^*$ | - | N | GiG | 0.0136 | 42.35 |
| NGC507$^*$ | 61.7 | N | IG | 0.0166 | 42.76 |
| NGC533$^*$ | 28.6 | N | GiG | 0.0157 | 42.29 |
| NGC708$^*$ | 65.7 | N | rG | 0.0136 | 43.09 |
| NGC741 | 478.8 | N | rG | 0.0151 | 41.79 |
| NGC777 | 7.0 | N | Sy2 | 0.0136 | 42.14 |
| NGC1399$^*$ | 208.0 | N | GiC | 0.0045 | 41.69 |
| NGC1404$^*$ | 3.9 | N | GiC | 0.0045 | 41.25 |
| NGC1407 | 87.7 | N | GiG | 0.0051 | 41.06 |
| NGC1550$^*$ | 16.6 | N | G | 0.0120 | 42.86 |
| NGC2300 | 2.9 | N | IG | 0.0069 | 41.22 |
| NGC2305 | - | S | G | 0.0114 | 41.73 |
| NGC2329 | 363.7 | N | rG | 0.0175 | 42.18 |
| NGC2340 | - | N | G | 0.0182 | 42.14 |
| NGC3091 | 2.5 | N | GiG | 0.0126 | 41.69 |
| NGC4073 | - | N | GiG | 0.0195 | 42.44 |
| NGC4203$^*$ | 6.1 | N | LIN | 0.0040 | 41.24 |
| NGC4261 | 4066.7 | N | LIN | 0.0078 | 41.27 |
| NGC4406$^*$ | - | N | GiC | 0.0040 | 42.11 |
| NGC4472$^*$ | 219.9 | N | Sy2 | 0.0040 | 41.49 |
| NGC4486$^*$ | 138487.0 | N | LIN | 0.0040 | 43.01 |
| NGC4636$^*$ | 77.8 | N | LIN | 0.0040 | 41.65 |
| NGC4649$^*$ | 29.1 | N | GiP | 0.0040 | 41.34 |
| NGC4696$^*$ | 5674.0 | S | GiC | 0.0092 | 43.29 |
| NGC4936 | 39.8 | N | LIN | 0.0102 | 41.75 |
| NGC5044$^*$ | 34.7 | N | GiG | 0.0075 | 42.80 |
| NGC5090 | 1325.8 | S | IG | 0.0105 | 41.55 |
| NGC5129 | 7.2 | N | GiG | 0.0224 | 42.20 |
| NGC5328 | - | N | GiC | 0.0152 | 41.94 |
| NGC5419 | 349.2 | N | rG | 0.0132 | 41.84 |
| NGC5846$^*$ | 21.0 | N | GiP | 0.0057 | 41.71 |
| NGC6407 | 54.6 | S | G | 0.0145 | 42.00 |
| NGC6868 | 138.8 | S | GiG | 0.0086 | 41.29 |
| NGC7049 | 93.2 | S | GiC | 0.0068 | 41.07 |
| NGC7619 | 20.3 | N | GiG | 0.0099 | 41.69 |
| Total | 34 | 42 | | | |

$^*$ - those galaxies in the detailed sample. The type-codes are as follows G-Galaxy, GiC-Galaxy in Cluster, GiG-Galaxy in Group, GiP-Galaxy in Pair, rG-Radio Galaxy, IG-Interacting Galaxy(ies), Sy2-Seyfert 2 galaxy, LIN-LINER-type Active Galaxy Nucleus. The surveys used are N-NVSS and S-SUMSS. $^a$ IC 2006 only has an upper limit on the X-ray luminosity so whether it is truly part of this sample is debatable. It also has no radio detection, and so it is possible that, given the high radio detection rate, that it has a much smaller X-ray luminosity than shown in the table.

## 8 LUMINOSITY FUNCTION

Fig. 11 shows the cumulative radio luminosity functions for the main and extended galaxy samples. The data $> 1 \times 10^{21}$ have been fitted with a simple Schechter function,

$$f_{\mathrm{radio-loud}} = f_0 \left(\frac{L}{L_*}\right)^{\alpha} \exp\left(\frac{L}{L_*}\right). \qquad (6)$$

A best fit results in $f_0 = 0.0289$, $\alpha = -0.367$ and $L_* = 7.79 \times 10^{24}$ W/Hz for the bins $> 1 \times 10^{21}$. Below around $\sim 2 \times 10^{21}$ W/Hz the function breaks again and can be modelled with a powerlaw of slope $-0.1$.

We also use the model used by Best et al. (2005)

$$f_{\mathrm{radio-loud}} = f_0 \left(\frac{M}{10^8 M_{\odot}}\right) \left[\left(\frac{L}{L_*}\right)^{\beta} + \left(\frac{L}{L_*}\right)^{\gamma}\right]^{-1}, \qquad (7)$$

---

[16] `http://simweb.u-strasbg.fr/simbad/`

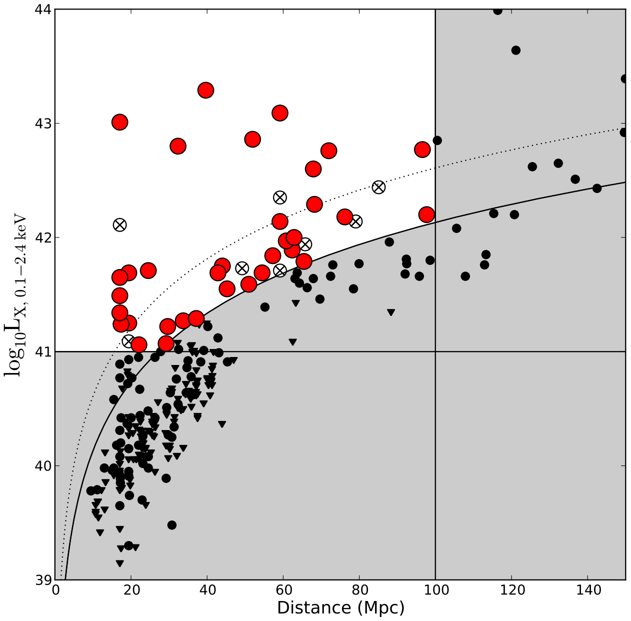

**Figure 10.** The distance-luminosity distribution of the galaxy sample of Beuing et al. 1999 with the lower flux cut and the luminosity cut used to create the extended sample. Those with detected radio emission in the NVSS or SUMSS have a red circle, those with no detection have a crossed,empty circle. We show the distance and X-ray luminosity limits, as well as the old (dotted) and new (solid) flux limits used to create this sample.

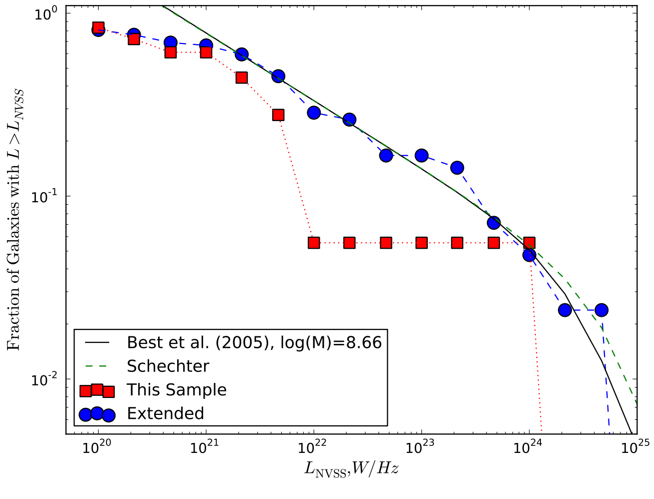

**Figure 11.** The luminosity functions of the main (red squares) and extended (blue circles) samples using the NVSS radio luminosities, supplemented by the SUMSS catalogue in the extended sample. We also show the best fit relation to the extended sample using both a Schechter function (green line) and the form of the luminosity function shown in Best et al. (2005) scaled for a mass of $10^{8.66}\,M_{\odot}$. as the solid black line.

where $f_0 = 3.5\times10^{-3}$, $\alpha = 1.6$, $\beta = 0.37$, $\gamma = 1.79$ and $L_* = 3.2\times10^{24}$ W/Hz but scaled for a mass of $10^{8.66}\,M_{\odot}$. In our study we have not split the sources by black hole mass, as in this case both samples are too small for this to be appropriate. Unsurprisingly the luminosity function is not very smooth, especially for the main sample presented in this paper. Despite this, the behaviour of the luminosity function of the radio galaxies shown in Best et al. (2005), with the break at around $10^{24}\mathrm{W/Hz}$, fits the luminosity function well.

When using both models, there appears to be evidence for a second break around $2\times10^{21}\,\mathrm{W/Hz}$, and the behaviour below this break appears to show that the fraction continues to rise towards one. This second break, if true, occurs at lower luminosities than those present in Best et al. (2005), but they do see a flattening of the luminosity function for the case of the most massive black hole bins.

Given the close agreement between the shapes of the luminosity functions presented here and in Best et al. (2005), the galaxies in our samples do not appear to be special – at least in their radio luminosities. Furthermore, given the comparatively few galaxies in our sample (42) compared to the many more in the SDSS study (2215) and the good agreement between the two shapes of the radio luminosity function, this implies that our sample is fairly unbiased to the radio luminosity of the galaxies within it.

## 9 CONCLUSIONS

Using a parent catalogue of elliptical galaxies with well determined optical properties we have identified a sample of 18 nearby, X-ray bright elliptical galaxies. Out of these 18 galaxies, 17/18 (94 per cent) have detected central radio emission and over half (10/18) have extended radio structures larger than 1 arcsecond. 12 galaxies have clear evidence for some disturbance of their X-ray halos, nine of which also have extended radio emission indicating a likely interaction of the radio and X-ray plasmas. Only two of the galaxies in our sample are above the radio loudness criterion of Best et al. (2005) (2/18, 11 per cent). However, the true level of radio activity is much higher. Extending the sample to lower X-ray fluxes, at the expense of data quality and completeness we find that 34/42 galaxies have a radio detection with the NVSS and SUMSS surveys. The lower sensitivity of these two surveys means this percentage should be regarded as a lower limit.

The mass-weighted cooling time within $1\,\mathrm{kpc}$ appears to anti-correlate with the total radio luminosity, particularly once systems for which the X-ray emission is dominated by nuclear point sources (IC 310 and NGC 4203) are excluded. This lends further support to the idea that hot gaseous halos of elliptical galaxies provide an important fuel source for the central AGN.

We have calculated upper limits on $k/f$, where $k$ is the ratio of the total particle energy to that of relativistic electrons radiating in the range of $10\,\mathrm{MHz}$ and $10\,\mathrm{GHz}$ and $f$ is the volume filling factor of the plasma in the cavity, for the extended radio lobes in the sample. The distribution of the upper limits on $k/f$ is broad and consistent with what would be expected as a radio plasma ages.

We calculate an X-ray radio loudness parameter for the total galactic emission in these two bands, $\mathcal{GR}_{\mathrm{X}}$. There is no clear correlation of $\mathcal{GR}_{\mathrm{X}}$ with the galaxy environment or $L_{\mathrm{X}}$.

## ACKNOWLEDGEMENTS

This research was supported by the DFG cluster of excellence Origin and Structure of the Universe (www.universe-cluster.de) and in part by the U.S. Department of Energy under contract number DE-AC02-76SF00515.

RJHD thanks the Alexander von Humboldt Foundation/Stiftung for financial support. SWA acknowledges support for this work from the National Aeronautics and Space Administration through Chandra Award Numbers AR7-8007X and G09-0088X. GBT acknowledges support for this work from the National Aeronautics and Space Administration through Chandra Award Number GO7-8124X issued by the Chandra X-ray Observatory Center, which is operated by the Smithsonian Astrophysical Observatory on behalf of the National Aeronautics and Space Administration under contract NAS803060A. GG is a postdoctoral researcher of the FWO-Vlaanderen (Belgium).

We thank Frazer Owen for the radio map of NGC 4486; Steve Rawlings and Paul Alexander for interesting discussions on $k/f$ and the anonymous referee whose suggestions improved this paper. This research has made use of the NASA/IPAC Extragalactic Data Base (NED) which is operated by the JPL, California Institute of Technology, under contract with the National Aeronautics and Space Administration.

## REFERENCES

Abell G. O., 1958, ApJS, 3, 211

Abell G. O., Corwin Jr. H. G., Olowin R. P., 1989, ApJS, 70, 1

Akritas M. G., Bershady M. A., 1996, ApJ, 470, 706

Allen S. W., Dunn R. J. H., Fabian A. C., Taylor G. B., Reynolds C. S., 2006, MNRAS, 372, 21

Arnaud K., 2004, in Bulletin of the American Astronomical Society Vol. 36 of Bulletin of the American Astronomical Society, XSPEC: Progress and Plans. pp 934–+

Arnaud K. A., 1996, in Jacoby G. H., Barnes J., eds, ASP Conf. Ser. 101: Astronomical Data Analysis Software and Systems V XSPEC: The First Ten Years. p. 17

Baldi A., Forman W., Jones C., Kraft R., Nulsen P., Churazov E., David L., Giacintucci S., 2009, 0904.2569

Balmaverde B., Capetti A., 2006, A&A, 447, 97

Becker R. H., White R. L., Helfand D. J., 1995, ApJ, 450, 559

Bender R., Capaccioli M., Macchetto F., Nieto J.-L., 1989, The Messenger, 55, 6

Best P. N., Kauffmann G., Heckman T. M., Brinchmann J., Charlot S., Ivezić Ž., White S. D. M., 2005, MNRAS, 362, 25

Best P. N., von der Linden A., Kauffmann G., Heckman T. M., Kaiser C. R., 2007, MNRAS, 379, 894

Beuing J., Dobereiner S., Bohringer H., Bender R., 1999, MNRAS, 302, 209

Biller B. A., Jones C., Forman W. R., Kraft R., Ensslin T., 2004, ApJ, 613, 238

Bîrzan L., McNamara B. R., Carilli C. L., Nulsen P. E. J., Wise M. W., 2007, in Böhringer H., Pratt G. W., Finoguenov A., Schuecker P., eds, Heating versus Cooling in Galaxies and Clusters of Galaxies Radio Properties of Cavities in the ICM: Imprints of AGN Activity. pp 115–+

Bîrzan L., McNamara B. R., Nulsen P. E. J., Carilli C. L., Wise M. W., 2008, ApJ, 686, 859

Birzan L., Rafferty D. A., McNamara B. R., Nulsen P. E. J., Wise M. W., 2009, in Heinz S., Wilcots E., eds, The Monsters' Fiery Breath The Detectability of AGN Cavities in Cooling-Flow Clusters

Bîrzan L., Rafferty D. A., McNamara B. R., Wise M. W., Nulsen P. E. J., 2004, ApJ, 607, 800

Blanton E. L., Sarazin C. L., McNamara B. R., Clarke T. E., 2004, ApJ, 612, 817

Bock D. C.-J., Large M. I., Sadler E. M., 1999, AJ, 117, 1578

Böhringer H., Voges W., Fabian A. C., Edge A. C., Neumann D. M., 1993, MNRAS, 264, L25

Bower R. G., Benson A. J., Malbon R., Helly J. C., Frenk C. S., Baugh C. M., Cole S., Lacey C. G., 2006, MNRAS, 370, 645

Brough S., Couch W. J., Collins C. A., Jarrett T., Burke D. J., Mann R. G., 2008, MNRAS, 385, L103

Brüggen M., Scannapieco E., Heinz S., 2009, MNRAS, 395, 2210

Buote D. A., Lewis A. D., Brighenti F., Mathews W. G., 2003a, ApJ, 594, 741

Buote D. A., Lewis A. D., Brighenti F., Mathews W. G., 2003b, ApJ, 595, 151

Burns J. O., 1990, AJ, 99, 14

Caon N., Macchetto D., Pastoriza M., 2000, ApJS, 127, 39

Capetti A., Balmaverde B., 2006, A&A, 453, 27

Carter B. J., Fabricant D. G., Geller M. J., Kurtz M. J., McLean B., 2001, ApJ, 559, 606

Cattaneo A., Faber S. M., Binney J., Dekel A., Kormendy J., Mushotzky R., Babul A., Best P. N., Brüggen M., Fabian A. C., Frenk C. S., Khalatyan A., Netzer H., Mahdavi A., Silk J., Steinmetz M., Wisotzki L., 2009, Nature, 460, 213

Chiaberge M., Capetti A., Macchetto F. D., 2005, ApJ, 625, 716

Churazov E., Brüggen M., Kaiser C. R., Böhringer H., Forman W., 2001, ApJ, 554, 261

Churazov E., Forman W., Jones C., Böhringer H., 2000, A&A, 356, 788

Churazov E., Sunyaev R., Forman W., Böhringer H., 2002, MNRAS, 332, 729

Clarke T. E., Blanton E. L., Sarazin C. L., Anderson L. D., Gopal-Krishna Douglass E. M., Kassim N. E., 2009, arXive/0903.0844

Colla G., Fanti C., Fanti R., Gioia I., Lari C., Lequeux J., Lucas R., Ulrich M. H., 1975, A&AS, 20, 1

Condon J. J., Cotton W. D., Greisen E. W., Yin Q. F., Perley R. A., Taylor G. B., Broderick J. J., 1998, AJ, 115, 1693

Croston J. H., Hardcastle M. J., Birkinshaw M., Worrall D. M., Laing R. A., 2008, MNRAS, 386, 1709

Croston J. H., Hardcastle M. J., Harris D. E., Belsole E., Birkinshaw M., Worrall D. M., 2005, ApJ, 626, 733

Croton D. J., Springel V., White S. D. M., De Lucia G., Frenk C. S., Gao L., Jenkins A., Kauffmann G., Navarro J. F., Yoshida N., 2006b, MNRAS, 367, 864

Croton D. J., Springel V., White S. D. M., De Lucia G., Frenk C. S., Gao L., Jenkins A., Kauffmann G., Navarro J. F., Yoshida N., 2006a, MNRAS, 365, 11

David L., Jones C., Giacintucci S., Forman W., Nulsen P., Vrtilek J., O'Sullivan E., Raychaudhury S., 2009, ArXiv e-prints

de Vaucouleurs G., de Vaucouleurs A., Corwin Jr. H. G., Buta R. J., Paturel G., Fouque P., 1991, Third Reference Catalogue of Bright Galaxies. Volume 1-3, XII, 2069 pp. 7 figs.. Springer-Verlag Berlin Heidelberg New York

de Vos M., Gunst A. W., Nijboer R., 2009, in Proceedings of the IEEE Vol. 97, The LOFAR Telescope, System Architecture and Signal Processing. pp 1431–1437

De Young D. S., 2006, ApJ, 648, 200

Di Matteo T., Allen S. W., Fabian A. C., Wilson A. S., Young A. J., 2003, ApJ, 582, 133

Dickey J. M., Lockman F. J., 1990, ARA&A, 28, 215

Dressler A., Thompson I. B., Shectman S. A., 1985, ApJ, 288, 481

Dunn R. J. H., Fabian A. C., 2004, MNRAS, 351, 862

Dunn R. J. H., Fabian A. C., 2006, MNRAS, 373, 959

Dunn R. J. H., Fabian A. C., 2008, MNRAS, 385, 757

Dunn R. J. H., Fabian A. C., Taylor G. B., 2005, MNRAS, 364, 1343

Ekers R. D., Kotanyi C. G., 1978, A&A, 67, 47

Ekers R. D., Wall J. V., Shaver P. A., Goss W. M., Fosbury R. A. E., Danziger I. J., Moorwood A. F. M., Malin D. F., Monk A. S., Ekers J. A., 1989, MNRAS, 236, 737

Ellingson S., Clarke T. E., Cohen A., Craig J., Kassim N. E., Philstrom Y., Rickard L. J., Taylor G. B., 2009, in Proceedings of the IEEE Vol. 97, The Long Wavelength Array. pp 1421–1430

Faber S. M., Wegner G., Burstein D., Davies R. L., Dressler A., Lynden-Bell D., Terlevich R. J., 1989, ApJS, 69, 763

Fabian A. C., Celotti A., Blundell K. M., Kassim N. E., Perley R. A., 2002, MNRAS, 331, 369

Fabian A. C., Sanders J. S., Allen S. W., Crawford C. S., Iwasawa K., Johnstone R. M., Schmidt R. W., Taylor G. B., 2003, MNRAS, 344, L43

Fabian A. C., Sanders J. S., Ettori S., Taylor G. B., Allen S. W., Crawford C. S., Iwasawa K., Johnstone R. M., Ogle P. M., 2000, MNRAS, 318, L65

Fabian A. C., Sanders J. S., Taylor G. B., Allen S. W., 2005, MNRAS, 360, L20

Fabian A. C., Sanders J. S., Taylor G. B., Allen S. W., Crawford C. S., Johnstone R. M., Iwasawa K., 2006, MNRAS, 366, 417

Ferrarese L., 2002, ApJ, 578, 90

Ferrarese L., Merritt D., 2000, ApJ, 539, L9

Filho M. E., Barthel P. D., Ho L. C., 2006, A&A, 451, 71

Finoguenov A., Pietsch W., Aschenbach B., Miniati F., 2004, A&A, 415, 415

Forman W., Jones C., Churazov E., Markevitch M., Nulsen P., Vikhlinin A., Begelman M., Böhringer H., Eilek J., Heinz S., Kraft R., Owen F., Pahre M., 2007, ApJ, 665, 1057

Forman W., Markevitch M., Jones C., Vikhlinin A., Churazov E., 2001, in Neumann D. M., Tran J. T. V., eds, Clusters of Galaxies and the High Redshift Universe Observed in X-rays New results from Chandra *

Forman W., Nulsen P., Heinz S., Owen F., Eilek J., Vikhlinin A., Markevitch M., Kraft R., Churazov E., Jones C., 2005, ApJ, 635, 894

Gallo E., Treu T., Jacob J., Woo J.-H., Marshall P. J., Antonucci R., 2008, ApJ, 680, 154

Gastaldello F., Buote D. A., Humphrey P. J., Zappacosta L., Bullock J. S., Brighenti F., Mathews W. G., 2007, ApJ, 669, 158

Gastaldello F., Buote D. A., Temi P., Brighenti F., Mathews W. G., Ettori S., 2009, ApJ, 693, 43

Goulding A. D., Alexander D. M., 2009, MNRAS, 398, 1165

Greisen E. W., 2003, in Heck A., ed., Astrophysics and Space Science Library Vol. 285 of Astrophysics and Space Science Library, AIPS, the VLA, and the VLBA. pp 109–+

Hardcastle M. J., Worrall D. M., Birkinshaw M., Canosa C. M., 2003, MNRAS, 338, 176

Hines D. C., Eilek J. A., Owen F. N., 1989, ApJ, 347, 713

Huchra J., Burg R., 1992, ApJ, 393, 90

Hudson M. J., Lucey J. R., Smith R. J., Schlegel D. J., Davies R. L., 2001, MNRAS, 327, 265

Humphrey P. J., Buote D. A., Brighenti F., Gebhardt K., Mathews W. G., 2008, ApJ, 683, 161

Iyomoto N., Makishima K., Matsushita K., Fukazawa Y., Tashiro M., Ohashi T., 1998, ApJ, 503, 168

Jones C., Forman W., Vikhlinin A., Markevitch M., David L., Warmflash A., Murray S., Nulsen P. E. J., 2002, ApJ, 567, L115

Kim D.-W., Fabbiano G., 1995, ApJ, 441, 182

Kim D.-W., Fabbiano G., 2004, ApJ, 611, 846

Kormendy J., 2001, in Cantó J., Rodríguez L. F., eds, Revista Mexicana de Astronomia y Astrofisica Conference Series Vol. 10 of Revista Mexicana de Astronomia y Astrofisica Conference Series, Supermassive Black Holes in Galactic Nuclei. pp 69–78

Kovalev Y. Y., Lister M. L., Homan D. C., Kellermann K. I., 2007, ApJ, 668, L27

Kraft R. P., Forman W. R., Churazov E., Laslo N., Jones C., Markevitch M., Murray S. S., Vikhlinin A., 2004, ApJ, 601, 221

Kriss G. A., Cioffi D. F., Canizares C. R., 1983, ApJ, 272, 439

Lauberts A., Valentijn E. A., 1989, The surface photometry catalogue of the ESO-Uppsala galaxies. Garching: European Southern Observatory, —c1989

Lonsdale C. J., MWA Collaboration 2007, in Bulletin of the American Astronomical Society Vol. 38 of Bulletin of the American Astronomical Society, The Murchison Widefield Array. pp 744–+

Machacek M., Dosaj A., Forman W., Jones C., Markevitch M., Vikhlinin A., Warmflash A., Kraft R., 2005, ApJ, 621, 663

Mauch T., Murphy T., Buttery H. J., Curran J., Hunstead R. W., Piestrzynski B., Robertson J. G., Sadler E. M., 2003, MNRAS, 342, 1117

McNamara B. R., Nulsen P. E. J., 2007, ARA&A, 45, 117

McNamara B. R., Wise M., Nulsen P. E. J., David L. P., Sarazin C. L., Bautz M., Markevitch M., Vikhlinin A., Forman W. R., Jones C., Harris D. E., 2000, ApJ, 534, L135

Mewe R., Kaastra J. S., Leidahl D. A., 1995, Legacy, 6, 16

Miller C. J., Nichol R. C., Gómez P. L., Hopkins A. M., Bernardi M., 2003, ApJ, 597, 142

Nagar N. M., Falcke H., Wilson A. S., 2005, A&A, 435, 521

Nulsen P. E. J., Jones C., Forman W. R., David L. P., McNamara B. R., Rafferty D. A., Bîrzan L., Wise M. W., 2007, in Böhringer H., Pratt G. W., Finoguenov A., Schuecker P., eds, Heating versus Cooling in Galaxies and Clusters of Galaxies AGN Heating Through Cavities and Shocks. pp 210–+

O'Sullivan E., Forbes D. A., Ponman T. J., 2001, MNRAS, 328, 461

O'Sullivan E., Vrtilek J. M., Kempner J. C., 2005, ApJ, 624, L77

Owen F. N., Eilek J. A., Kassim N. E., 2000, ApJ, 543, 611

Paolillo M., Fabbiano G., Peres G., Kim D.-W., 2003, ApJ, 586, 850

Piffaretti R., Jetzer P., Kaastra J. S., Tamura T., 2005, A&A, 433, 101

Rafferty D. A., McNamara B. R., Nulsen P. E. J., Wise M. W., 2006, ApJ, 652, 216

Randall S., Nulsen P., Forman W. R., Jones C., Machacek M., Murray S. S., Maughan B., 2008, ApJ, 688, 208

Randall S. W., Sarazin C. L., Irwin J. A., 2004, ApJ, 600, 729

Richstone D., 1998, in Sofue Y., ed., The Central Regions of the Galaxy and Galaxies Vol. 184 of IAU Symposium, Black holes and galaxy centers (Review). pp 451–+

Rickes M. G., Pastoriza M. G., Bonatto C., 2004, A&A, 419, 449

Sanders J. S., Fabian A. C., 2002, MNRAS, 331, 273

Santra S., Sanders J. S., Fabian A. C., 2007, MNRAS, 382, 895

Shurkin K., Dunn R. J. H., Gentile G., Taylor G. B., Allen S. W., 2008, MNRAS, 383, 923

Sijbring D., de Bruyn A. G., 1998, A&A, 331, 901

Somerville R. S., Hopkins P. F., Cox T. J., Robertson B. E., Hernquist L., 2008, MNRAS, 391, 481

Stanger V. J., Warwick R. S., 1986, MNRAS, 220, 363

Stoughton C., Lupton R. H., Bernardi M., Blanton M. R., Burles S., Castander F. J., Connolly A. J., Eisenstein D. J., Frieman J. A., Hennessy G. S., 2002, AJ, 123, 485

Sun M., 2009, 0904.2006

Sun M., Forman W., Vikhlinin A., Hornstrup A., Jones C., Murray S. S., 2003, ApJ, 598, 250

Taylor G. B., Fabian A. C., Allen S. W., 2002, MNRAS, 334, 769

Taylor G. B., Sanders J. S., Fabian A. C., Allen S. W., 2006, MNRAS, 365, 705

Terashima Y., Wilson A. S., 2003, ApJ, 583, 145

Trinchieri G., Goudfrooij P., 2002, A&A, 386, 472

Tully R. B., 1988, Nearby galaxies catalog. Cambridge and New York, Cambridge University Press, 1988, 221 p.

Vernaleo J. C., Reynolds C. S., 2006, ApJ, 645, 83

York D. G., Adelman J., Anderson Jr. J. E., Anderson S. F., Annis J., Bahcall N. A., Bakken J. A., Barkhouser R., Bastian S., Berman E., 2000, AJ, 120, 1579

Young A. J., Wilson A. S., Mundell C. G., 2002, ApJ, 579, 560